AGU ADVANCING EARTH AND SPACE SCIENCES

Water Resources Research

RESEARCH ARTICLE
10.1029/2025WR040838

Young Versus Old: Does Forest Age Regulate Water and Dissolved Carbon Processes Belowground?

Fiona S. Liu[1], Devon Kerins[1,2], Shreya Ramesh[3], Pamela L. Sullivan[4], Sharon A. Billings[5], Daniel R. Hirmas[6], Hoori Ajami[7], Alejandro Flores[8], Catalina Segura[9], and Li Li[1]

[1]Department of Civil and Environmental Engineering, The Pennsylvania State University, University Park, PA, USA, [2]School of Civil Engineering, University College Dublin, Dublin, Ireland, [3]Department of Earth Sciences, University of Southern California, Los Angeles, CA, USA, [4]College of Earth, Ocean, and Atmospheric Sciences, Oregon State University, Corvallis, OR, USA, [5]Department of Ecology and Evolutionary Biology, Kansas Biological Survey & Center for Ecological Research, University of Kansas, Lawrence, KS, USA, [6]Department of Plant and Soil Science, Texas Tech University, Lubbock, TX, USA, [7]Department of Environmental Sciences, University of California Riverside, Riverside, CA, USA, [8]Department of Geosciences, Boise State University, Boise, ID, USA, [9]Department of Forest Engineering, Resources, and Management, Oregon State University, Corvallis, OR, USA

Key Points:

- Higher vertical connectivity in an old forest promoted deep flow contributions and sustained more baseflow compared to a young forest
- Dissolved carbon concentrations are higher in old forests than young ones, mainly produced in shallow subsurface, peaking in summers
- Forest age is important but insufficient to predict the export patterns of DOC

Supporting Information:

Supporting Information may be found in the online version of this article.

Correspondence to:

L. Li and F. S. Liu,
lxl35@psu.edu;
fsl5026@psu.edu

Citation:

Liu, F. S., Kerins, D., Ramesh, S., Sullivan, P. L., Billings, S. A., Hirmas, D. R., et al. (2026). Young versus old: Does forest age regulate water and dissolved carbon processes belowground? *Water Resources Research*, *62*, e2025WR040838. https://doi.org/10.1029/2025WR040838

Received 18 APR 2025
Accepted 12 DEC 2025

Abstract Forest plantations are widespread globally. Young forest plantations (hereafter young forests) differ from natural old-growth forests (hereafter old forests) in above- and below-ground structures, shaping water and carbon cycling processes. While above-ground differences are well studied, below-ground hydrology and biogeochemical processes remain poorly understood. Here we asked: *How do hydrological flow paths and dissolved carbon processes belowground differ between young and old forests?* Using a process-based hydro-biogeochemical model (BioRT-HBV) constrained by streamflow and dissolved organic and inorganic carbon (DOC and DIC) data, we analyzed three pairs of young-old forests at the H.J. Andrews Experimental Forest, Oregon, USA. Detailed simulations for a 57-year-old plantation (WS01) and a naturally regenerated ~500-year-old forest (WS02) showed that the young forest had lower streamflow and smaller deep groundwater contributions (20%) than the old forest (30%). DOC was mainly produced in shallow soil but diverged with depth: transformed into DIC in the young forest and further produced in the old forest, yielding contrasting export patterns of flushing (DOC increases with discharge) and dilution (DOC decreases with discharge). These differences likely stem from variations in subsurface structures, supported by deeper, denser roots in old forest. Extending the analysis to two additional pairs showed (a) higher DOC and DIC concentrations in all old forests; (b) consistent DIC dilution patterns but variable DOC patterns. Numerical experiments indicate that these diverse DOC behaviors result from interactions among forest age, geology, and hydrological connectivity, and other factors, highlighting the overlooked role of forest development in subsurface carbon cycling.

Plain Language Summary Clear-cutting followed by replanting has created many forest plantations around the world. These forests differ from older, naturally regenerated forests above and below the surface, where water and carbon move through soil and rock. However, we still know relatively little about how these belowground processes differ between younger and older forests and how they influence stream water chemistry. In this study, we used a computer model (BioRT-HBV) with streamflow and water chemistry data from the H.J. Andrews Experimental Forest in Oregon, USA, focusing on two important water quality components, dissolved organic carbon (DOC) and dissolved inorganic carbon (DIC), which play key roles in carbon cycling and ecosystem health. We compared a younger, 57-year-old plantation with an older, ~500-year-old forest to examine how water movement and dissolved carbon processes vary with forest age. We found that the older forest had stronger vertical connections, allowing more water and carbon to move through deep soil layers and sustaining streamflow from groundwater. In contrast, the younger forest had shallower flow paths and less deep carbon production. Streams draining older forests contained higher dissolved carbon overall, showing how differences in subsurface structure shape water quality and carbon cycling in changing forests.

1. Introduction

Forests play a vital role in regulating global carbon and water cycles (Dudley & Stolton, 2003; Harris et al., 2021), yet their structure and function are increasingly altered by land use change and forest management (Curtis et al., 2018; Hansen et al., 2013). In response to rising timber demand and forest conservation policies, forest plantations and naturally regenerating forests are replacing old-growth forests at an accelerating rate (Du

et al., 2022; Holl & Brancalion, 2020; UNEP & FAO, 2020). As of 2020, forest plantations alone occupy approximately 7% of the global forest area (UNEP & FAO, 2020).

Studies of the carbon dynamics at different successional stages (i.e., young vs. mature or old) has proliferated for decades (e.g., McGrath et al., 2024; Nave et al., 2025; Odum, 1969). Young forests often display high net primary productivity as carbon is preferentially allocated to biomass gain; in contrast, old forests often appear to shift investment toward structural stability, with relatively slower biomass increment (Litton et al., 2007; Pregitzer & Euskirchen, 2004; Ryan et al., 1997). Young forests, whether regenerating naturally following disturbance or established through plantation forestry, differ structurally and functionally from old forests that have developed over centuries with minimal disturbance. Forest plantations are often characterized by even-aged trees, dense planting, and uniform species compositions due to commercial management practices (Bauhus, 2009; Carle & Vuorinen, 2002). In contrast, old forests often contain mixed-age trees, and more complex canopy structures, and often exhibit more stable ecosystem functions that contribute to long-term carbon storage and water supply (Lindenmayer & Bowd, 2022; Oliver & Larson, 1996).

Much of these studies focus on above-ground processes, although these differences also extend below-ground, influencing soil structure, root systems, and subsurface processes. Old forests tend to support thicker organic layers, greater root densities, and more extensive deep root networks compared to young forests (Bauhus, 2009; Billings et al., 2018; Hertel et al., 2003; Yanai et al., 2006). Deep roots enhance access to deep water reserves, supporting transpiration and carbon uptake during dry periods (Pivovaroff et al., 2021; Tao et al., 2021; Zhang et al., 2017). Old forests have also shown higher soil CO_2 efflux (Campbell & Law, 2005; Rodtassana et al., 2021) and elevated concentrations of dissolved organic carbon in streams (Cawley et al., 2014; Fegel et al., 2021; Hood et al., 2006; Meyer & Tate, 1983; Smiley & Trofymow, 2017). In contrast, young forests often exhibit reduced streamflow and altered hydrological dynamics due to differences in canopy interception, transpiration, and flow routing (Crampe et al., 2021; Perry & Jones, 2017; Segura et al., 2020). Young forests have been observed to typically retain limiting nutrients efficiently through tight cycling tied to growth demand (Vitousek & Reiners, 1975), whereas old forests approach a more conservative, steady-state condition of internal nutrient retention (Valett et al., 2002).

These observations underscore the need to better understand the differences in hydrology and carbon processes below young and old forests that ultimately affect streamflow generation, water quality, and carbon cycling. Subsurface structure, in particular, often regulates the transformation and transport of solutes such as dissolved organic and inorganic carbon (DOC and DIC) from terrestrial to aquatic systems (Stewart et al., 2024; Wen et al., 2022). High DOC concentrations in streams can cause water browning (Blanchet et al., 2022), mobilize toxic elements (Römkens et al., 1999; Zhao et al., 2007), and form harmful disinfection byproducts during drinking water treatment (Leonard et al., 2022; Sadiq & Rodriguez, 2004). Meanwhile, DIC regulates stream pH, buffering capacity, and riverine CO_2 outgassing to the atmosphere (Grandi & Bertuzzo, 2022; Marx et al., 2017; Tank et al., 2018).

Subsurface data are generally collected using lysimeters, groundwater wells, hydrometric and isotopic measurements, and soil-groundwater monitoring, which have provided valuable insights into subsurface flow paths and solute generation (Laudon et al., 2011; Ledesma et al., 2015). However, subsurface measurements have remained labor-intensive and limited in spatial and temporal coverage. Concentration-discharge (CQ) relationships measured in streams can be used as integrative indicators of hydrological and biogeochemical processes and solute sources at the catchment scale (Rose et al., 2018; Stewart, Shanley, et al., 2022; Zhi et al., 2019). DOC typically follows a flushing pattern, where concentrations increase with discharge (Herndon et al., 2015; Sebestyen et al., 2009; Zarnetske et al., 2018), reflecting the mobilization of DOC-rich shallow soil water during high-flow events at high hydrological connectivity (Raymond & Saiers, 2010; Stewart & Li, 2025; Ågren et al., 2007). DIC often shows a dilution pattern, where concentrations decrease with discharge, as DIC-rich deep soil waters are diluted by low-DIC shallow inputs during high flows (Najjar et al., 2020; Stewart, Zhi, et al., 2022; Wallin et al., 2013).

Subsurface structure and processes are essential in shaping these CQ patterns. For instance, carbon cycling occurring at depth beneath soils (deep respiration) is increasingly recognized as a critical, yet often overlooked, component of catchment carbon budgets (Harper & Tibbett, 2013; Hasenmueller et al., 2017; Tune et al., 2020). Deep respiration has been shown to lead to the widely observed flushing pattern for DOC and dilution pattern for DIC (Kerins et al., 2024; Stewart et al., 2024). Storm-driven changes in flow paths can further modify CQ

patterns, sometimes resulting in dilution instead of the expected flushing for DOC (Knapp et al., 2020; Su et al., 2023). In high-elevation mountains with permafrost, CQ patterns of DIC transitioned from dilution in colder years to chemostasis (relatively constant concentration) in warmer years, possibly due to enhanced soil respiration and weathering during permafrost thawing (Xu et al., 2024).

While these studies contribute to a growing body of literature on the importance of subsurface structure in determining water and dissolved carbon dynamics in subsurface, the influence of forest successional stages has remained poorly understood. Here we ask the question: *Does forest age regulate belowground water and carbon processes? How do hydrological flow paths and dissolved carbon processes (transformation and transport) differ between young and old forests?* We address this question by comparing a young and old forest at H.J. Andrews Experimental Forest. We hypothesize that *deeper and denser root systems in old forests promote vertical connectivity and DOC production at depth, leading to distinct concentration discharge relationships that differ from those in young forests.* To test this hypothesis, we compared three pairs of adjacent young-versus-old forests in the H.J. Andrews Experimental Forest (Oregon, USA): WS01-02, WS06-08, and WS09-10. WS01, WS06, and WS10 are young forests with plantations established after clear-cutting in 1960–1970s, whereas WS02, WS08, and WS09 are old forests with ages of 150–500 years. These pairs share similar climate but differ in geology and topography (Swanson, 1975). We leverage streamflow (Johnson et al., 2024) and stream chemistry data (Johnson & Fredriksen, 2019a, 2019b) at these intensively measured catchments to constrain a reactive transport model, BioRT-HBV (Sadayappan et al., 2024) and to understand water and dissolved carbon cycling (production and export, or transformation and transport). We focused model calibration and process analysis on the WS01 and WS02 pair because these two sites have subsurface root data; without subsurface data for other sites, we used numerical thought experiments to explore the factors driving difference across all catchments.

2. Methods

2.1. Study Site

The H.J. Andrews Experimental Forest (HJA), established in 1943, is located in the Willamette National Forest of the western Cascade Mountains, Oregon, USA. It is managed by the U.S. Forest Service as part of its experimental forest network and has been part of the Long-Term Ecological Research (LTER) program since 1980. The forest was originally established to study impacts of forest management practices on catchment-scale processes, particularly in relation to water quality, quantity, and vegetation succession (Johnson et al., 2021).

We focus the modeling on a paired set of headwater catchments: an experimental catchment (WS01) and a reference catchment (WS02). Both are steep, small basins (<1 km^2) situated at low-elevations (440–800 m), with WS01 (0.96 km^2) slightly larger than WS02 (0.60 km^2) (Figure 1). The region has an orographically influenced Mediterranean climate, with warm, dry summers and cold, wet winters (Rothacher, 1970). Mean annual precipitation is 2,200 mm with 75% occurring from November to April. Mean daily air temperature reaches 18°C in July and 2°C in December. Snowpack rarely persists for more than a few weeks (Johnson et al., 2021). The geology consists of highly weathered Oligocene tuffs and breccias (Swanson, 1975). Soils of these two catchments are mapped predominantly as Dutchoven (loamy-skeletal, isotic, mesic Andic Humudepts; J. Winter, personal communication) and Kinney (fine-loamy, isotic, mesic Andic Humudepts) complexes (Soil Survey Staff, 2024).

Before timber harvest, both catchments were dominated by 450-year-old Douglas-fir (*Pseudotsuga menziesii*) forests (Dyrness, 1973; Johnson & Jones, 2000). Between 1962 and 1966, WS01 underwent 100% clear-cutting using cable logging without road construction, minimizing soil erosion and mass wasting (Goodman et al., 2023). The logged area was subsequently broadcast burned (Johnson & Jones, 2000) and replanted with Douglas-fir seedlings (Jones & Grant, 1996). Today, this young WS01 is a 57-year-old Douglas-fir plantation (Bingham & Jr.Sawyer, 2022). In contrast, WS02 remained unharvested and free of major disturbances in recent centuries. It is dominated by native Douglas-fir trees ranging from 150 to over 500 years old, which regenerated after wildfires in the early 1,500s and mid-1,800s (Perry & Jones, 2017; Weisberg & Swanson, 2003). Both catchments, however, were affected by severe wildfires that burned portions of HJA in 2020.

Two other young-old catchment pairs exist at HJA, WS06-08 and WS09-10, that have been monitored for stream chemistry. Similar to WS01 and WS02, the young forests (WS06 and WS10) were fully clear-cut and replanted in 1975 and now are ~50-year-old trees. Their paired old forests (WS08 and WS09) represent unharvested reference

10.1029/2025WR040838

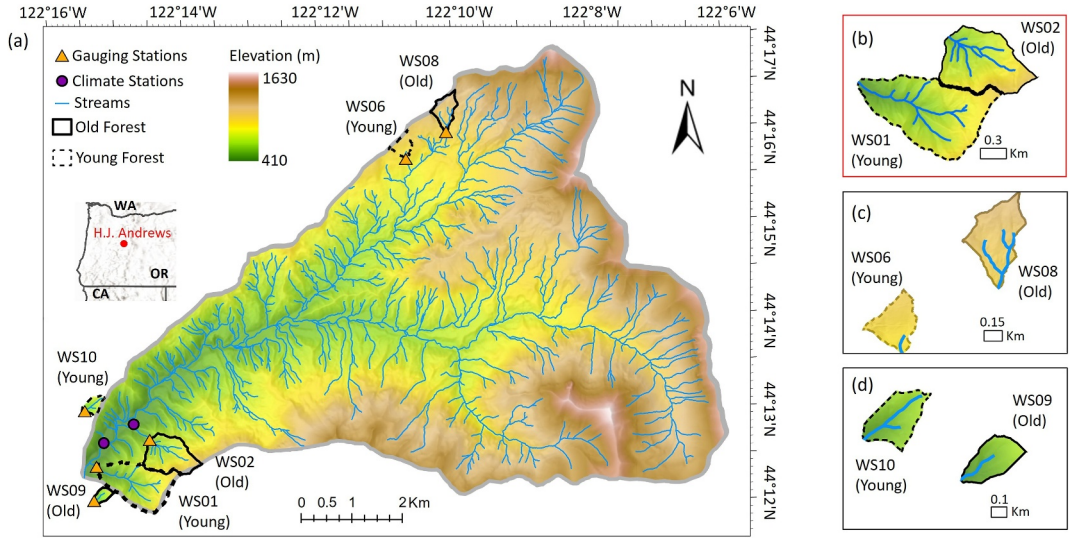

Figure 1. (a) Map of the H.J. Andrews Experimental Forest in Oregon, USA, showing the locations of the three young–old forest pairs. Old forest areas are outlined in black, and young forest are outlined with black dashed lines. Triangles indicate stream gauging stations used for streamflow and chemistry data collection, while circles denote climate stations used for model calibration. Panels (b–d) show the three study catchment pairs: (b) WS01 (young) and WS02 (old), (c) WS06 (young) and WS08 (old), and (d) WS09 (old) and WS10 (young). The red outline in panel (b) highlights the WS01 and WS02 pair, which served as the primary focus of model calibration.

sites. These additional pairs, however, differ from WS01 and WS02 in catchment size, geology, slope, elevation, and snow regimes (see Table S1 in Supporting Information S1 for detailed catchment characteristics). For instance, WS06 and WS08 are located in the upper elevations of HJA, which receive higher annual precipitation and maintain seasonal snowpacks, whereas the other two pairs lie in lower elevations where snow rarely persists beyond a few weeks. The upper sites are underlain by Miocene andesitic basalt flows, while the lower sites consist of highly weathered Oligocene tuffs and breccias (Swanson, 1975). Among these, WS06 also contains road cover (Johnson et al., 2021).

2.2. Data

Daily air temperature and precipitation data were obtained from the Primary Meteorological Station (PRIMET) for WS01 and the Climatic Station at Watershed 2 (CS2MET) for WS02 (Daly et al., 2019). Precipitation chemistry data were derived from wet deposition samples collected at the PRIMET station (Johnson & Fredriksen, 2019a) and applied to both catchments. Samples were shipped to and analyzed for a broad suite of solutes by the Cooperative Chemical Analytical Laboratory (CCAL, Oregon State University, Corvallis, OR). Details of analytical instrumentation, methods, and standard operating procedures are available at http://www.ccal.oregonstate.edu/. Potential evapotranspiration (PET) was estimated using long-term daily air temperature data (1980–2017) and the Hargreaves and Samani equation (Hargreaves & Samani, 1985), implemented with the R package "Evapotranspiration" (Guo et al., 2016).

Daily stream discharge (Johnson et al., 2024) and chemistry data (available every 3 weeks) were obtained from their respective stream gauge stations located at the outlets of each catchment (Johnson & Fredriksen, 2019b). Composite water samples are collected and analyzed about every 3 weeks (Fredriksen, 1969, 2019) therefore representing time-integrated composite of stream water chemistry over 3-week periods. This composite sampling introduces some limitations to our analyses. Composite samples can mask important dynamics in stream chemistry, including short-term responses to individual storm events or rapid biogeochemical shifts, which are often critical for understanding and simulating catchment scale processes. The temporal averaging may also reduce the variation in concentrations that are central to CQ patterns. However, these limitations mean that any detectable differences in stream water chemistry across these paired watersheds using composite samples reflect meaningful, broad differences in generalizable patterns useful for addressing our hypothesis.

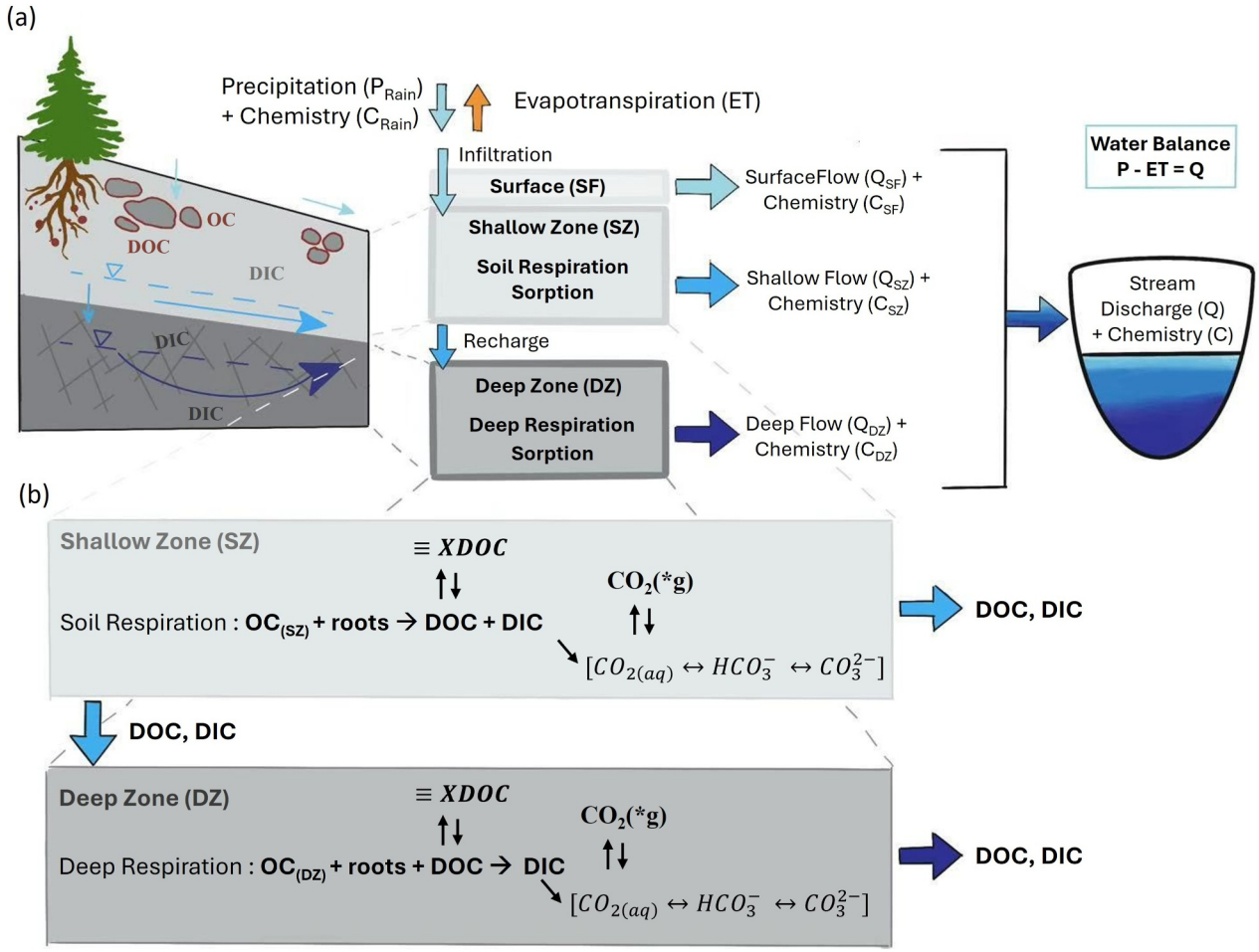

Figure 2. (a) A conceptual diagram of the BioRT-HBV reactive transport model, representing the catchment as comprising of three buckets: a surface/topsoil (SF) with rapid flow Q_{SF}, a shallow zone (SZ) with intermediate flow Q_{SZ}, and a deeper zone (DZ) with slow flow Q_{DZ}. The Q_{SF}, Q_{SZ}, and Q_{DZ} are Q_0, Q_1, and Q_2 in the HBV model, respectively. (b) Reaction networks implemented in this work include soil respiration in the SZ, deep respiration in the DZ, DOC sorption on the surfaces of soils/rocks and gas-aqueous CO_2 exchange processes in both zones. "$OC_{(SZ)}$" and "$OC_{(DZ)}$" represent soil organic carbon in the SZ and DZ, respectively, while "≡ XDOC" denotes sorbed DOC on soil surfaces. Details of reactions and key calibrated parameters are in Table 1.

2.3. BioRT-HBV Overview

2.3.1. HBV Model

BioRT-HBV is a catchment-scale reactive transport model that integrates the hydrological HBV model with the BioRT reactive transport framework (Sadayappan et al., 2024). The HBV module simulates hydrological processes, including snow accumulation and melting, soil moisture dynamics, and runoff responses (Bergström, 1976; Seibert & Vis, 2012). It conceptualizes a catchment as two stacked upper and lower buckets and three flow paths (Figure 2). These buckets and flow paths are not assigned explicit depths as they can vary depending on the characteristics of specific catchments. They represent average, "effective" shallow and deep subsurface zones that contribute different "effective" flows to streams and rivers. These effective dynamics emerge from the complexity and connectivity of subsurface structures and manifest at the scale of entire catchments.

Each bucket represents a water storage compartment that can be broadly characterized as a shallow soil zone and a deeper groundwater zone. These conceptualizations are based on assumptions that reflect observations from field studies. The shallow zone is often associated with shallow subsurface with weathered soils and high clay and organic matter content, unsaturated conditions, fluctuating interflow, and relatively fast flow (Sullivan et al., 2016; Torres et al., 2015). In contrast, the deep zone is associated with deeper subsurface, strongly

influenced by parent rock (Frisbee et al., 2013), generally saturated with slower flow, and older water that sustains baseflow during low-flow periods. These zones collectively generate three flow pathways represented in the HBV model as (a) the quick flow Q_0, representing rapid flow above the ground surface and/or at topsoil (Q_{SF}); (b) the intermediate flow Q_1 from shallow soil zone flow (Q_{SZ}); and (c) the slow flow Q_2 representing groundwater flow from deep zones (Q_{DZ}).

Total water storage in each zone includes dynamic storage, the portion that actively contributes to streamflow (Soulsby et al., 2011) and passive storage, the portion that supports vegetation and biogeochemical reactions. Passive storage cannot be differentiated by hydrometeorological observations (Kirchner, 2009) and is calibrated within the reactive transport model. The HBV model is driven by catchment-scale daily inputs of precipitation, air temperature, and PET. The model partitions the total precipitation into evapotranspiration (ET) and streamflow, the latter coming from the land via three components: surface, shallow, and deep flow paths. The magnitude of each flow depends on hydrometeorological conditions and the internal characteristics of the bucket, which depends on its water storage and related parameters that determine each flow. The model generates daily hydrologic outputs, which include evapotranspiration (ET), streamflow, dynamic water storage from each zone, and the three flow components (surface, shallow and deep flow).

2.3.2. BioRT Model

The BioRT module uses HBV outputs (water storage and flow components) to simulate solute transport and biogeochemical reactions at the catchment scale. Reaction networks are implemented in both the shallow and the deep zones, where mass conservation equations are solved for dissolved solutes. Reactions in the surface zone are not explicitly modeled in this work, as rapid surface flow typically provides insufficient residence time for biogeochemical transformation. However, surface (overland) flow can interact with leaf litter and organic-rich surficial soils, contributing additional DOC to streams (Johnson et al., 2006; Lee & Lajtha, 2016; Meyer et al., 1998; Ryan et al., 2021). To account for this contribution, DOC concentrations in the surface zone were assumed to be twice those in the shallow zone, representing enhanced leaching of organic matter from the litter layer and forest floor, following Stewart and Li (2025), who derived this assumption from synthesis of multiple field data sets across forested catchments. In contrast, DIC concentrations in the surface zone were assumed to be near zero, reflecting equilibrium with atmospheric CO_2. Model outputs include daily solute concentrations and reaction rates for each zone, and stream solute concentrations at the catchment outlet.

The governing equations for mass conservation of an arbitrary solute i are as follows:

Surface Zone (SF):

$$\frac{d(C_{SF,i}V_{w,SF})}{dt} = P_{\text{rain}}C_{\text{rain},i} - Q_{SF}C_{SF,i} - Q_{infil}C_{infil,i} \tag{1}$$

where $V_{w,SF}$ [mm] is the water volumes in the surface zone; P_{rain} [mm d^{-1}] is the daily rainfall amount; $C_{\text{rain},i}$; $C_{infil,i}$,; $C_{SF,i}$ [mol L^{-1}] are the concentrations of solute i in rainfall, infiltration water, and the surface zone, respectively; Q_{infil}, and Q_{SF} [mm d^{-1}] are the water fluxes infiltrating into the shallow soil zone and move into streams from the surface zone. $C_{infil,i}$ [mol L^{-1}] is derived from precipitation chemistry as: $C_{infil,i} = \frac{P_{\text{rain}} \times C_{\text{rain},i}}{(P_{\text{rain}} - ET)}$ because ET does not return chemicals back to the atmosphere but rather leaves them behind in the remaining water. Snow can also contribute to infiltration chemistry. However, at low elevations of HJA, snowpack rarely persists for more than a few weeks such that $C_{infil,i}$ is primarily governed by precipitation chemistry.

Shallow Soil Zone (SZ):

$$\frac{d(C_{SZ,i}V_{w,SZ})}{dt} = Q_{infil}C_{infil} - (Q_{SZ} + Q_{Perc})\,C_{SZ,i} + R_{SZ,i} \tag{2}$$

Deep Zone (DZ):

$$\frac{d(C_{DZ,i}V_{w,DZ})}{dt} = Q_{Perc}C_{SZ,i} - Q_{DZ}C_{DZ,i} + R_{DZ,i} \tag{3}$$

In Stream Mixing:

$$C_{\text{stream}}(t) = \frac{Q_{SF}(t)\,C_{SF,i}(t) + Q_{SZ}(t)\,C_{SZ,i}(t) + Q_{DZ}(t)\,C_{DZ,i}(t)}{Q_{SF}(t) + Q_{SZ}(t) + Q_{DZ}(t)} \quad (4)$$

Here $C_{SZ,i}$, and $C_{DZ,i}$ [mol L^{-1}] are the concentrations of solute i in shallow soil and deep zones, respectively. $V_{w,SZ}$ and $V_{w,DZ}$ [mm] are the water volumes in the shallow soil and deep zones, respectively. Q_{Perc}, Q_{SZ}, and Q_{DZ} [mm d^{-1}] are the water fluxes from the water recharging into the deep zone and the flows from the shallow soil zone and the deep zone to streams, respectively. Both water volumes and water fluxes are normalized by the drainage areas. Lastly, $R_{SZ,i}$ and $R_{DZ,i}$ [mol m^{-2} d^{-1}] are the overall reaction rates for solute i in the shallow soil and deep zones. Multiple reactions can occur in each zone such that the reaction rates are the summation of all reaction rates for solute i.

2.4. Reactions

2.4.1. Reaction Networks

Soil organic carbon comprises an array of compounds that are chemically diverse and challenging to characterize explicitly (Lehmann & Kleber, 2015; Schmidt et al., 2011). We simplify this complexity by representing soil organic carbon as a generic organic carbon (OC_{SZ}) pool. A portion of this pool undergoes mineralization via heterotrophic respiration, producing CO_2. During this process, OC_{SZ} is also decomposed into smaller, more soluble molecules, generating dissolved organic carbon (DOC), which can be further respired to become CO_2 gas. Some fractions of the CO_2 can dissolve in water and become CO_2 (aq), entering the carbonic acid system and contributing to the dissolved inorganic carbon (DIC) pool (Reaction 1a). BioRT further accounts for direct DOC inputs from plant root exudates and the contribution of CO_2(aq) through autotrophic root respiration (Reaction 1b). However, due to the inherent difficulty in distinguishing autotrophic and heterotrophic sources of DOC and CO_2(aq) (Hanson et al., 2000), these processes are aggregated into a single, shallow-zone soil respiration network. This net reaction (Reaction 1) lumps the production of DOC and CO_2(aq) from $OC_{(SZ)}$ via multiple reactions pathways, as well as the respiration of DOC to CO_2(aq).

Additionally, DOC can bind to soil through sorption, particularly under conditions of high concentrations of clay minerals that provide abundant surface area for sorption (Mayes et al., 2012). In BioRT, sorption is represented as an equilibrium-controlled reaction (Reaction 2), where the extent of DOC binding is governed by an equilibrium constant (K_{eq}) that dictates the balance between concentrations of DOC in water and soil or rock surfaces in shallow and deep zones. However, the sorption capacity in the deep zone is expected to be lower than in the shallow zone, as the deep zone represents weathered and fractured bedrock materials with limited clay and reactive mineral surfaces compared to the overlying soils (Kaiser & Guggenberger, 2000).

DOC in the shallow zone can percolate downward with recharge, introducing fresh carbon sources and fueling microbial respiration at depth (Fontaine et al., 2007). Older, slow-turnover carbon in the deep zone can also undergo decay and subsequent respiration, even with lower oxygen availability (Fang & Moncrieff, 2005). The generally longer residence times of deeper water facilitate the gradual breakdown of this slow-turnover carbon pool (Tune et al., 2020). Together, these old and translocated carbon sources form the basis for another "net" reaction of DOC production and consumption in the deep zone. This is conceptualized as a deep-zone respiration in the model (Reaction 3), which accounts for two primary carbon pools: an older, slow-turnover organic carbon pool (OC_{DZ}) and DOC inputs from the shallow zone, both contributing to DIC production through microbial mineralization.

Shallow and deep respiration produce CO_2, which undergoes gas-aqueous exchange governed by Henry's Law and CO_2(aq) solubility (Marx et al., 2017). This exchange is modeled through a conceptual CO_2(*g) block, representing an immobile, residual phase of CO_2(g) trapped within soil pores that can dissolve into CO_2(aq) (Reaction 4). Depending on pH, CO_2(aq) rapidly dissociates to form other carbonate species, including bicarbonate (HCO_3^-), and carbonate (CO_3^{2-}) (Reactions 5 and 6). The DIC is the sum of all three solutes.

2.4.2. Rate Laws

The rates of respiration reactions are assumed to depend on temperature and soil moisture in the form:

$$r = kAf(T)f(S_w) \tag{5}$$

where r is the reaction rate [mol s^{-1}], k is the kinetic reaction rate constant [mol m^{-2} s^{-1}], and A is the reactive surface area [m^2] that depend on reactive materials such as organic carbon, root abundance, and microbial community. The functions $f(T)$ and $f(S_w)$ account for temperature and soil moisture effects, respectively (Davidson et al., 1998). Due to a lack of direct measurements for electron donors and acceptors, reaction rates are treated as effective rates, capturing the combined influence of multiple donor and acceptor sources. The framework does not explicitly incorporate limiting substrate factors but assumes a sufficient supply of soil organic carbon as electron donors and diverse potential electron acceptors. Variations in the utilization of these acceptors are indirectly captured through the soil moisture function, which modulates reaction rates in response to changing hydrological conditions.

Rates of microbial activity and carbon decomposition generally increase with temperature (Davidson & Janssens, 2006; Li et al., 2024). We used the widely used Q_{10} form (Lloyd & Taylor, 1994):

$$f(T) = Q_{10}^{(T-20)/10} \tag{6}$$

Here, Q_{10} represents the relative rate increase for every 10°C rise in temperature, typically ranging from 1.0 to 3.0 depending on site-specific conditions such as climate and land cover (Mahecha et al., 2010; Zhou et al., 2009).

Optimal soil moisture is crucial for regulating microbial activity and respiration rates: while adequate moisture promotes aerobic decomposition, excess moisture limits oxygen availability (Yan et al., 2018). We used the soil moisture function $f(S_w)$ as follows:

$$f(S_w) = \begin{cases} \left(\frac{S_w}{S_{w,c}}\right)^n, S_w \le S_{w,c} \\ \left(\frac{1-S_w}{1-S_{w,c}}\right)^n, S_w > S_{w,c} \end{cases} \tag{7}$$

Here, $S_{w,c}$ is the critical soil moisture at which respiration rates peak. When $S_w \le S_{w,c}$, respiration rates increase with S_w; when $S_w > S_{w,c}$, respiration rates decline due to reduced oxygen availability in saturated soils. The exponent n adjusts the sensitivity of reaction rates to soil moisture, typically ranging from 1.0 to 3.0 depending on soil properties such as structure and texture (Hamamoto et al., 2010).

The rates of CO_2 gas-aqueous exchange process are approximated using Transition State Theory (TST) rate law (Lasaga, 2014):

$$r = kA\left(1 - \frac{IAP}{K_{eq}}\right) \tag{8}$$

here, r is the reaction rate [mol s^{-1}], k is the rate constant [mol m^{-2} s^{-1}], and A is the effective surface area of the pseudo solid-phase CO_2(*g) undergoing mimicked weathering [m^2 m^{-3}]. *IAP* represents the ion activity product, and K_{eq} is the equilibrium constant. The ratio *IAP* to *Keq* indicates the deviation from equilibrium, which in turn determines the reaction's directionality.

2.5. Model Calibrations

2.5.1. HBV

We employed the Genetic Algorithm and Powell (GAP) optimization tool (Seibert, 2000) to calibrate HBV hydrological parameters against observed streamflow data for water years (WY) 2015–2017, using WY2014 as a spin-up period to stabilize initial conditions. This calibration period was selected because it provided continuous discharge and forcing data and encompassed a range of hydrologic regimes. Annual discharge totals were higher in WY2016 and WY2017 compared to WY2015, reflecting wetter conditions that coincided with the strong 2015–2016 El Niño event.

The GAP framework combines a global genetic algorithm with local refinement by the Powell method (Okamoto et al., 1998; Seibert, 2000). Each trial begins with a population of randomly selected parameter values, with ranges predefined based on prior HBV applications (Beck et al., 2016; Karimi et al., 2022; Seibert & McDonnell, 2010). Model performance was evaluated using three objective functions: Nash-Sutcliffe Efficiency (NSE) to assess fit to peak flows, NSElog to assess fit to low flows, and Volume Error (VE) to assess fit to annual discharge volumes. For all three metrics, values closer to 1 indicate better model performance (See Text S1 in Supporting Information S1 for metric equations). The best-performing parameter sets were retained as parents and recombined across successive generations, mimicking natural selection and progressively improving model fit. Once promising parameter sets are identified, the Powell algorithm was applied to fine-tune solutions and converge toward local optima that best represented observed streamflow.

For each catchment, 200 GAP trials were performed, producing 200 parameter sets capable of reproducing streamflow, achieving NSE values >0.7. In addition, stream chemistry data provided an independent constraint on hydrology and flow path partitioning. Because unrealistic flow partitioning cannot reproduce observed DOC and DIC dynamics (Kerins et al., 2024; Stewart et al., 2024), this additional layer of evaluation increased confidence in the selected parameter sets and robustness of the GAP calibration results.

2.5.2. BioRT

We calibrated the BioRT model using stream chemistry data. Because direct measurements of DIC were unavailable, we calculated stream DIC concentrations from measured pH and alkalinity following Wolf-Gladrow et al. (2007). Alkalinity, defined as $C_{HCO_3^-} + 2(C_{CO_3^{2-}}) + C_{OH^-}$, represents the water's capacity to neutralize acid with carbonate species concentrations. Using $C_{CO_{2(aq)}} = \frac{C_{H^+} + C_{HCO_3^-}}{K_1}$ and $C_{CO_3^{2-}} = \frac{K_2\ C_{HCO_3^-}}{C_{H^+}}$, where $K_1 = 10^{-6.35}$ and $K_2 = 10^{-10.33}$ at 25°C and standard atmospheric pressure, DIC was calculated as $C_{DIC} = C_{HCO_3^-}\left(\frac{C_{H^+}}{K_1} + \frac{K_2}{C_{H^+}} + 1\right)$. Although this method can overestimate DIC under acidic conditions (Abril et al., 2014), the relatively neutral pH range (7.0–8.1) in the streams here minimize this concern.

We selected the HBV case with streamflow partitioning closest to the mean of the 200 GAP trials for the hydrologic inputs in the BioRT model. BioRT calibration was then conducted through a stepwise manual process, where reactions were added sequentially and parameters iteratively adjusted to reproduce measured stream DOC and DIC concentrations. To match the HJA sampling schedule, daily model outputs were aggregated into 3-week flux intervals, upon which model performance was evaluated using NSE and KGE.

2.6. Model Uncertainty Analysis

For hydrology, the acceptable HBV cases from the GAP trials converged on a relatively narrow range of flow partitioning, all of which showed high performance with NSE >0.7. This convergence is tighter than what has been reported in HBV applications in sites with more snow, where acceptable parameter sets produced a wider range of flow path partitioning (Kerins et al., 2024; Stewart et al., 2024), possibly because time series of streamflow data in rain-dominated WS01 and WS02 provide more nuanced information than those in snow-dominated catchments where streamflow from snowmelt often obscure the time stamps of precipitation. For BioRT calibration, we used the HBV case that most closely reflected the mean flow partitioning across all acceptable runs. To further explore the effects of hydrologic uncertainty, this mean case was evaluated alongside two additional HBV cases that represented the maximum and minimum fractions of deep flow (Q_{DZ}%) observed among the acceptable GAP runs.

To assess potential equifinality in the BioRT module, we also conducted a sensitivity analysis using Latin Hypercube Sampling (Helton & Davis, 2003). For each catchment, 5,000 parameter sets were generated across an expanded parameter range informed by the manual calibration process. These parameter sets were tested with the three selected HBV cases (minimum, mean, and maximum Q_{DZ}%), resulting in 30,000 simulations across the two catchments. However, none of these randomly generated parameter sets achieved NSE values above zero for stream DOC and DIC, reinforcing our reliance on the manual calibration process. This outcome is consistent with previous BioRT applications (Kerins et al., 2024; Stewart et al., 2024) and likely arise from the high interdependence of different reactions and non-linearity of rate laws. Even with a relatively small number of reactions, strong interdependencies among reactions and solutes in different zones, coupled with nonlinear kinetics and

Table 1
Reaction Networks and Key Calibration Parameters for the BioRT Model

Reaction name "label"	Reaction network	Rate law	Logk [mol m^{-2} s^{-1}]	$logK_{eq}$	SSA [m^2 g^{-1}]	Q_{10}	$S_{w,c}$	$S_{w,n}$
Reactions in Shallow Zone (SZ)								
(1) Soil Respiration "Resp-SZ"	$OC_{(SZ)}$ + roots → 0.40[a]DOC + 0.5[b]DIC	Equation 5[c]	−10.0	–	0.1 (*0.08*)	2.1 (*2.3*)	0.5 (*0.4*)	0.8
(1a) Heterotrophic Respiration	$OC_{(SZ)}$ → DOC + DIC	–	–	–	–	–		–
(1b) Autotrophic Respiration	Roots → DIC	–	–	–	–	–		–
Reactions in Deep Zone (DZ)								
(2) Deep Respiration "Resp-DZ"	$OC_{(DZ)}$ + DOC → 0.7[d]DIC (*$OC_{(DZ)}$ → DOC + 0.8[e]DIC*)[f]	Equation 5[c]	−11.0	–	0.8 (*9.0*)	1.0	0.8 (*0.7*)	1.2 (*1.5*)
Reactions in both Shallow and Deep Zones								
(3) DOC Sorption[g] "Sorption"	≡XDOC ↔ ≡X + DOC	Equilibrium[h]	–	−0.20	–	–	–	–
(4) CO_2 Gas-Aqueous Exchange* "CO_2(*g)"	CO_2(*g) ↔ $CO_{2(aq)}$	TST[i]	−13.1	−2.92	SZ: 0.1	SZ: 0.6	SZ: 0.6 (*0.7*)	SZ: 0.7 (*0.6*)
					DZ: 0.001	DZ: 1.2 (*1.0*)	DZ: 1.0	DZ: 1.0
(5) CO_2 Speciation	$CO_{2(aq)}$ + H_2O ↔ HCO_3^- + H^+	Equilibrium[h]	–	−6.35	–	–		–
(6) HCO_3 Speciation	HCO_3^- ↔ H^+ + CO_3^{2-}	Equilibrium[h]	–	−10.33	–	–		–

Note. Parameters were calibrated separately for the young (WS01) and old (WS02) forest based on measured stream DOC and DIC concentrations. For parameters with identical values in both catchments, only one value is listed; for those that differ, the old forest value is provided in *italics (in parentheses)*. $OC_{(SZ)}$ and $OC_{(DZ)}$ denote the soil organic carbon pools in the shallow soil zone (SZ) and deep zone (DZ), respectively. Other reactants and products include soil sorption sites (≡X), sorbed DOC (≡XDOC), and CO_2(*g), which represents the immobile, residual phase of CO_2(g) trapped within soil pores that can dissolve into CO_2(aq). SSA refers to the specific surface area of reactive materials used to calculate the reactive surface area (A) in the reaction rate laws. Q_{10} indicates the factor by which the reaction rate increases for every 10°C rise in temperature. Superscript letters in the reaction networks denote calibrated stoichiometric coefficients. [a]DOC partitioning from shallow respiration (0.4 DOC). [b]DIC partitioning from shallow respiration (0.5 DIC). [c]see Equation 5. [d]DIC partitioning from deep respiration (0.7 DIC). [e]DIC partitioning from deep respiration in the old forest (0.8 DIC). [f]Reaction network for deep respiration in the old forest modified to yield a net DOC production in the deep zone. Three rate law forms are used. [g]For the sorption reaction, logKeq is identical across zones, but the initial concentration of sorption sites (X-) differs between SZ and DZ to represent reduced sorption capacity in the deep zone. (See Table S6 in Supporting Information S1 for additional model parameters). [h]Equilibrium (thermodynamically controlled and reversible), and. [i]TST = Transition State Theory (see Equation 8).

thermodynamic constraints, narrows the parameter space that can reproduce observations. This highlights the importance of incorporating modeler expertise to guide parameterization, particularly in representing how flow partitioning and reaction processes jointly control solute concentrations.

2.7. Catchment Scale Production and Export Rates

BioRT simulates daily reaction rates for kinetically controlled processes in shallow and deep zones. These rates are multiplied by the corresponding stoichiometric coefficients (Table 1) to calculate the daily production rates (R_p) of DOC and DIC in each zone. For each solute, total production rates are obtained by summing up the production and consumption rates across all kinetic reactions involving that solute. Daily export rates (R_e) were calculated by summing up the product of dissolved carbon concentrations and their corresponding water fluxes from each zone at the daily scale.

2.8. Root Abundance Data

Subsurface water chemistry data were not available for WS01 and WS02. To qualitatively assess the modeled results, we leveraged root abundance data representing vertical profiles of coarse and fine root presence from soil pits excavated in WS01 (young) and WS02 (old). Each soil pit was dug to a depth of 1 m, and vertical faces were carefully cleaned to expose undisturbed soil and roots before being photographed. High-resolution photos were overlaid with a 1 × 1 cm grid, and each cell was analyzed for the presence or absence of coarse roots (diameter ≥ 1 mm) and fine roots (diameter < 1 mm). When both root types were present in a cell, only coarse root presence were recorded due to their larger volume and stronger influence on soil structure (Billings et al., 2018; Jarecke et al., 2025). Presence/absence data were aggregated into 5-cm depth intervals and expressed as the

fraction of each 5-cm-thick soil layer containing roots. Statistical differences in median root fractions between the young and old forests were evaluated separately for coarse and fine roots in the shallower (<50 cm) and deeper (≥50 cm) soil layers using the non-parametric Mann–Whitney U test in R (R Core Team, 2024). A depth of 50 cm was chosen as an approximate midpoint of the soil profiles to separate shallower and deeper soil layers.

2.9. Numerical Thought Experiment for Other Young and Old Catchments

In addition to WS01 (young) and WS02 (old), two other young-old catchment pairs (WS06-WS08 and WS09-WS10) have been monitored for stream chemistry (Johnson & Fredriksen, 2019b). These pairs differ from WS01 and WS02 in catchment size, elevation, geology, and snow regime (see Section 2.1). To investigate whether differences in subsurface hydrology and reactivity, beyond those explained by forest age, could account for the variability in DOC and DIC CQ patterns across these catchments, we conducted a series of numerical thought experiments using the calibrated WS01 model as a baseline configuration. Five variables were systematically evaluated separately for their influence on the concentrations, depth profiles, and CQ patterns of dissolved carbon: (a) hydrological partitioning (Q_{DZ}%), where the proportion of discharge routed through the deep zone was varied between 10% and 50% of total flow, encompassing and extending beyond the modeled range for WS01 and WS02 and representing potentially different subsurface physical structures (soil and rock and root characteristics) in other forests; (b) deep zone carbon reaction types with three scenarios: net production (+DOC), no net reaction (0DOC), and net consumption (–DOC); (c) rates of deep zone consumption (-DOC), where rate constants were varied (0.5x, 1x, and 2x of the calibrated model baseline) to represent conditions with differing microbial activity and substrate availability; (d) rates of deep zone production (+DOC), where rate constants were varied (0.5x, 1x, and 2x of the calibrated model baseline) to simulate enhanced DOC generation from deeper organic sources and roots; and (e) rates of shallow zone production (+DOC), where rate constants were varied (0.5x, 1x, and 2x of the calibrated model baseline) to assess the influence of soil carbon dynamics.

Together, these modifications produced a suite of numerical experiments representing distinct combinations of subsurface flow partitioning and reaction conditions. This design allowed us to isolate and evaluate how hydrological connectivity and biogeochemical reactivity can control the concentrations and export patterns of dissolved carbon in subsurface and in streams draining forests of different ages.

3. Results

3.1. Distinct Streamflow and Flow Partitioning in WS01 and WS02

Streamflow exhibited strong seasonal variability in both catchments, with high flows during cool, wet winters and low flows in warm, dry summers (Figure 3). In the young forest, total annual streamflow averaged 1,013 ± 292 mm yr^{-1} over the study period, with notable interannual variability; in the old forest, annual totals averaged 1,243 ± 360 mm yr^{-1}. Their corresponding runoff ratios (Q/P) are 0.46 and 0.54, respectively, indicating a higher proportion of precipitation to streamflow in the old forest. Seasonal contrasts were particularly pronounced. In the young forest, winter streamflow averaged 430 ± 140 mm compared to only 13 ± 6 mm in summer. Similarly, in the old forest, winter flows averaged 510 ± 180 mm, while summer flows averaged 37 ± 13 mm. On average, annual streamflow in the young forest was 18.5% lower than in the old forest, and the difference was even greater during the summer months, reaching up to 45% lower.

The HBV model effectively captured the seasonal dynamics, achieving high performance at NSE values of 0.75 ± 0.01 and 0.72 ± 0.01 in the young and old forests, respectively. NSElog was higher, averaging 0.90 ± 0.01 for both catchments, and volume error performance was strong (VE = 0.99), indicating an almost identical match between modeled and observed total streamflow. Shallow soil flow (Q_{SZ}) was predominant, responding rapidly to precipitation events and driving most of the storm hydrograph. Deep groundwater flow (Q_{DZ}) supplied the remainder, providing relatively steady contributions during events and sustaining baseflow during dry summer months. The main difference between the two catchments is in the subsurface flow partitioning. In the young forest, Q_{SZ} accounted for 79 ± 1.2% of annual streamflow and Q_{DZ} 19 ± 1.2%, whereas in the old forest Q_{SZ} accounted for 69 ± 2.5% and $Q_{DZ.}$ 29 ± 3.5%. Over the 3-year simulation period, the old forest received an average of 365 ± 46 mm yr^{-1} from deep groundwater, nearly double the 197 ± 13 mm yr^{-1} estimated for the young forest.

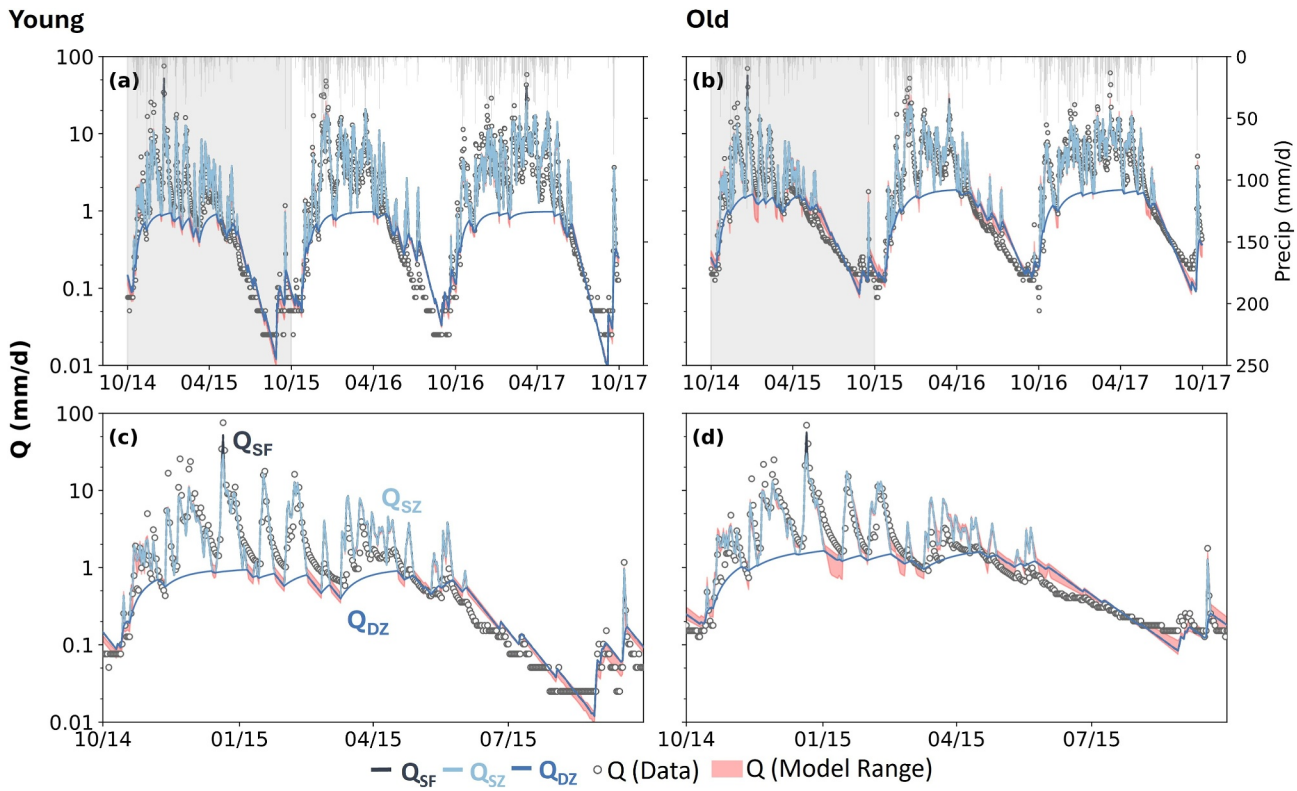

Figure 3. (a, b) Timeseries of daily streamflow data (gray circles), measured precipitation (top, Gy bars), and model outputs for the young and old forests over WY2015-2017. Modeled flow partitioning is shown as additive components: surface flow (Q_{SF}, black), shallow soil flow (Q_{SZ}, light blue), and deep groundwater flow (Q_{DZ}, dark blue), which together sum to total simulated stream discharge. Note that Q_{SF} is very small (<2%) and is largely invisible. The range of GAP simulation trials is shown as a pink band; where the band is not visible, it closely matches the plotted lines and is therefore difficult to distinguish. (c, d) Zoomed view of WY2015 highlighting the uncertainty range from GAP trials (pink band), alongside observed stream discharge and modeled flow partitioning. Q_{SZ} dominates the annual hydrograph and responds rapidly to precipitation, whereas Q_{DZ} provides sustained baseflow through seasonal wet and dry periods.

3.2. Contrasting Stream Carbon Export Patterns

Stream dissolved carbon concentrations exhibited seasonal patterns in both catchments. In the young forest, DOC concentrations peaked at approximately 2.6 mg L^{-1} following the first few precipitation events during the transition from the warm, dry season to the cool, wet season and then declined as streamflow increased. During the dry season, DOC concentrations dropped to around 0.9 mg L^{-1} (Figure 4b). In contrast, DIC concentrations displayed opposite patterns. DIC concentrations rose steadily during the dry season, reaching a peak of approximately 7.9 mg L^{-1}, and declined during the wet season as streamflow increased, reaching a baseline value of 4.3 mg L^{-1} (Figure 4f). These seasonal dynamics were reflected in the CQ relationships, where DOC showed a weak flushing tendency, with concentrations increasing slightly with discharge (slope = 0.07, R^2 = 0.18, p = 0.002; Figure 4a), while DIC followed a dilution pattern, with concentrations decreasing with flow (slope = −0.10, $R^2 = 0.92$, $p < 0.001$; Figure 4e). These weak patterns with relatively low b values likely, at least partially, resulted from the composite water sampling that averaged water chemistry over 3-week periods.

In the old forest, DOC concentrations showed seasonal patterns distinct from those in the young. While DOC still peaked during seasonal transitions, peak values were higher, reaching around 3.7 mg L^{-1}. Notably, DOC concentrations in the old forest displayed an unusual rise during the dry season, culminating in a seasonal high just before the onset of the wet season. The lowest DOC concentrations, approximately 0.95 mg L^{-1}, occurred during the wet months of March and April (Figure 4d). The DOC CQ relationships in the old forest revealed a dilution pattern (slope = −0.18, $R^2 = 0.42$, $p < 0.001$; Figure 4c). DIC patterns in the old forest were consistent with those in the young, showing increases during the dry season and decreased during the wet seasons, aligned with a dilution CQ pattern (slope = −0.13, $R^2 = 0.93$, $p < 0.001$; Figure 4g). Peak DIC concentrations reached around 6.84 mg L^{-1}, with lows around 3.95 mg L^{-1} in the wet season (Figure 4h).

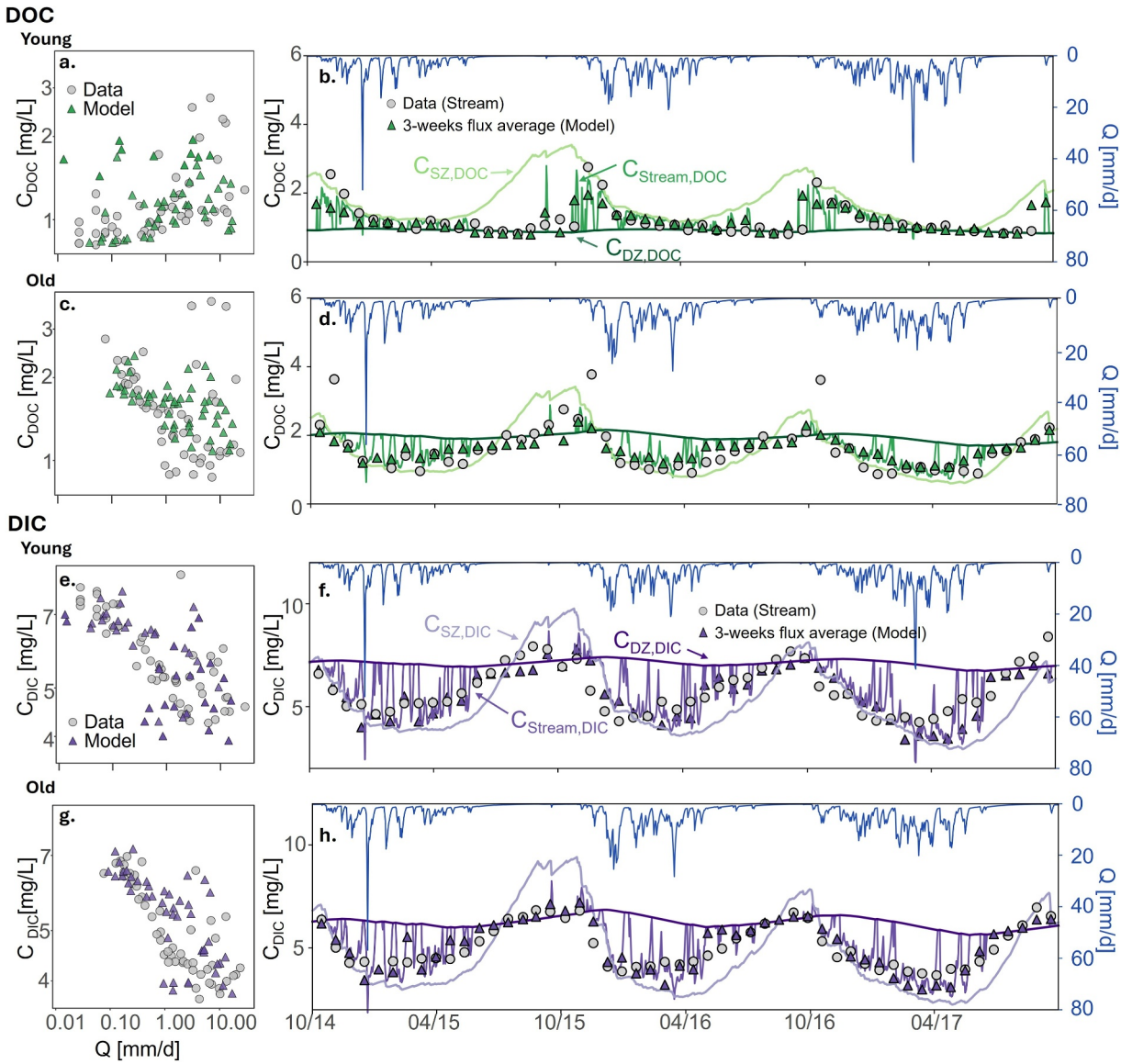

Figure 4. Left: Concentration-discharge (CQ) relationships of observed stream data (circles) and 3-week flux averages from model outputs (triangles) for DOC in the (a) young and (c) old forest, and DIC in the (e) young and (g) old forest. Right: Corresponding time series of observed stream concentration data (circles), modeled concentrations in the stream, shallow zone (SZ), and deep zone (DZ), along with 3-week flux averages from model outputs of DOC in the (b) young and (d) old forest, and DIC in the (f) young and (h) old forest. Regression statistics indicate that the young forest exhibited a weak flushing DOC CQ pattern, whereas the old forest showed a strong dilution DOC pattern. DIC exhibited a dilution pattern in both watersheds.

The BioRT model captured the temporal patterns and the directionality of the CQ relationships for DOC and DIC in both catchments. For DOC, the model achieved NSE values of 0.42 (young) and 0.48 (old), and KGE values of 0.55 and 0.46, respectively. For DIC, the model performed was higher, achieving NSE values of 0.62 (young) and 0.69 (old), and KGE values of 0.81 and 0.83, respectively.

3.3. Subsurface Depth Profiles: Modeled Dissolved Carbon Consistent With Root Data

Modeled DOC concentrations varied with depth between the young and old forests (Figure 5a). In the shallow zone (SZ), DOC concentrations were similar across the two forests, indicating comparable production in soil. In contrast, in the deep zone (DZ), modeled DOC concentrations were higher in the old forest, suggesting enhanced production. Root abundance data provides qualitative support for these modeled depth profiles (Figure 5b). Root distributions differed substantially between the young and old forests, particularly in the deeper soil layers

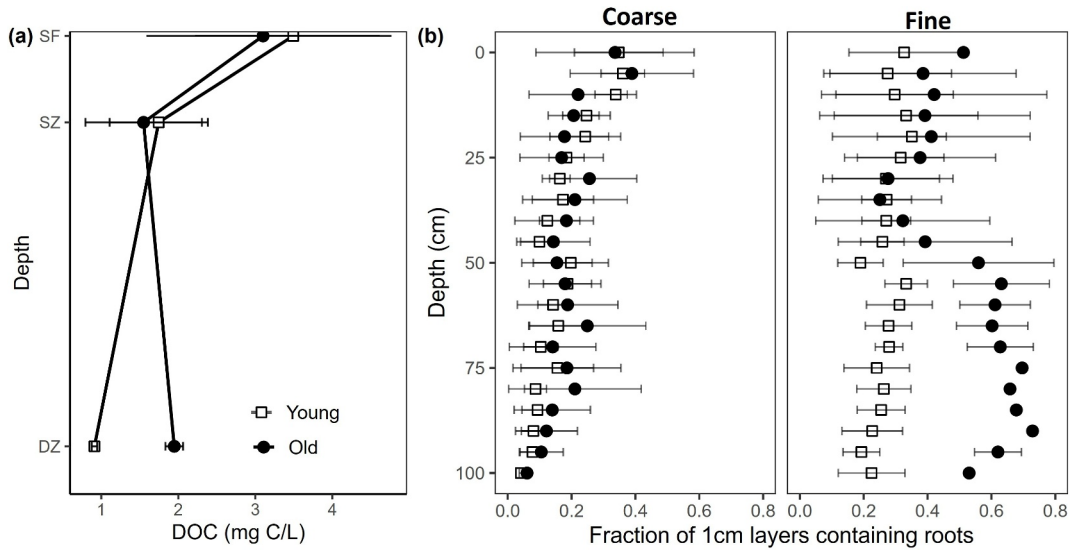

Figure 5. (a) Modeled DOC concentrations along the depth profile, indicating higher DOC accumulation in the deep zone (DZ) in the old forest. (b) Depth distribution of coarse and fine root fractions, showing a greater abundance of fine roots at depth in the old forest (black circles) compared to the young forest (white squares). These patterns collectively illustrate the link between enhanced DOC production at depth and the deeper, more connected root system in the old forest.

(≥50 cm). Coarse roots were generally more abundant in the shallow soil (<50 cm) and declined with depth in both catchments. Coarse root abundance was not significantly different between the two forests in shallow subsurface ($p = 0.74$) but was significantly different at depth ($p < 0.05$) with a higher fraction of coarse roots in the old forest. The contrast was more pronounced for fine roots: in the young forest, fine roots were distributed relatively evenly with depth, whereas in the old forest, fine root abundance increased markedly in deeper layers. Differences in fine root abundance between the two forests were marginal in shallow soils ($p = 0.46$) but highly significant at depth ($p < 0.001$).

3.4. Production and Export Rates

In the young forest, mean DOC production rate ($R_{P,\ DOC}$) was 3.2 ± 2.8 mg m^{-2} d^{-1}, primarily driven by shallow zone production at 3.6 ± 2.8 mg m^{-2} d^{-1} with the deep zone acting as a net consumer (−0.4 ± 0.02 mg m^{-2} d^{-1}; Figure 6e, green). Shallow zone DOC production responded strongly to rising air temperatures, peaking at 6.6 ± 2.4 mg m^{-2} d^{-1} during the summer. Mean DIC production rate ($R_{P,\ DIC}$) was 11.7 ± 3.2 mg m^{-2} d^{-1}, with most production occurring in the shallow zone (10.5 ± 3.2 mg m^{-2} d^{-1}) and only a minor contribution (1.2 ± 0.1 mg m^{-2} d^{-1}) from the deep zone (Figure 6e, purple). $R_{P,\ DIC}$ also peaked in summer at 14.8 ± 2.4 mg m^{-2} d^{-1}.

In contrast, the old forest exhibited greater overall DOC production, with the deep zone playing a more substantial role (Figure 7). Mean $R_{P,\ DOC}$ was 4.3 ± 2.9 mg m^{-2} d^{-1}, split between shallow zone production (3.7 ± 2.9 mg m^{-2} d^{-1}) and a notable deep zone contribution (0.6 ± 0.05 mg m^{-2} d^{-1}; Figure 6f, green). This contrasted with the young forest, where the deep zone acted as a net DOC consumer. Summer $R_{P,\ DOC}$ peaked at 8.2 ± 2.3 mg m^{-2} d^{-1}, exceeding that of the young forest. Mean $R_{P,\ DIC}$ reached 13.0 ± 2.1 mg m^{-2} d^{-1}, with 10.7 ± 2.0 mg m^{-2} d^{-1} from the shallow zone and 2.3 ± 0.1 mg m^{-2} d^{-1} from the deep zone (Figure 6f, purple). $R_{P,\ DIC}$ also peaked during the summer at 14.9 ± 2. mg m^{-2} d^{-1}. Overall, the old forest demonstrated higher dissolved carbon production, with its deep zone making a more prominent contribution in comparison to the young forest.

Export rates (R_e) were closely tied to streamflow patterns, reflecting seasonal flow dynamics. In the young forest, mean $R_{e,\ DOC}$ was 3.5 ± 5.2 mg m^{-2} d^{-1}, largely from the shallow zone (3.0 ± 5.0 mg m^{-2} d^{-1}), with the deep zone contributing a smaller but steady 0.5 ± 0.3 mg m^{-2} d^{-1} (Figure 6g, green). $R_{e,\ DOC}$ peaked in the winter at 7.3 ± 6.7 mg m^{-2} d^{-1}. Mean $R_{e,\ DIC}$ was 13.1 ± 16.9 mg m^{-2} d^{-1}, dominated by the shallow zone

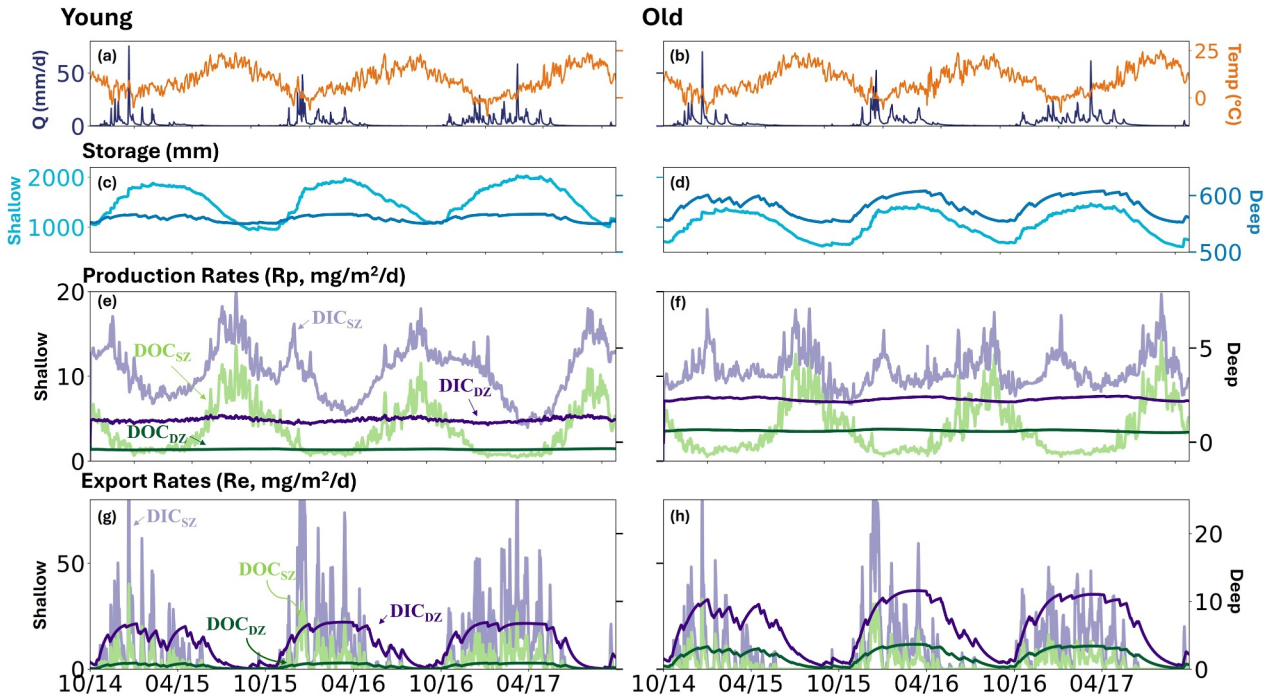

Figure 6. (a, b) Time series of streamflow (blue) and air temperature (orange) data for the young and old forest. (c, d) Modeled water storage in the shallow zone (SZ) and deep zone (DZ). (e, f) Modeled daily production rates (R_p) and (g, h) export rates (R_e) of DOC (green) and DIC (purple) from the SZ and DZ. Secondary *y*-axes in panels (e–h) highlight magnitude differences between the SZ and DZ. R_p peaks during the summer, while R_e peaks during the wet winter periods. The old forest exhibits higher R_p and R_e for both DOC and DIC, driven by greater contributions from DZ.

(9.2 ± 15.4 mg m^{-2} d^{-1}) with additional inputs from the deep zone (3.9 ± 2.4 mg m^{-2} d^{-1}; Figure 6g, purple). Peak winter exports reached 26.2 ± 20.6 mg m^{-2} d^{-1}.

The old forest again showed higher overall export rates, particularly due to greater contributions from the deep zone. Mean $R_{e,\,DOC}$ was 4.6 ± 5.1 mg m^{-2} d^{-1}, with contributions of 2.6 ± 5.1 mg m^{-2} d^{-1} from the shallow zone and 2.0 ± 1.2 mg m^{-2} $d^{-1}$from the deep zone (Figure 6h, green). $R_{e,\,DOC}$ peaked in winter at

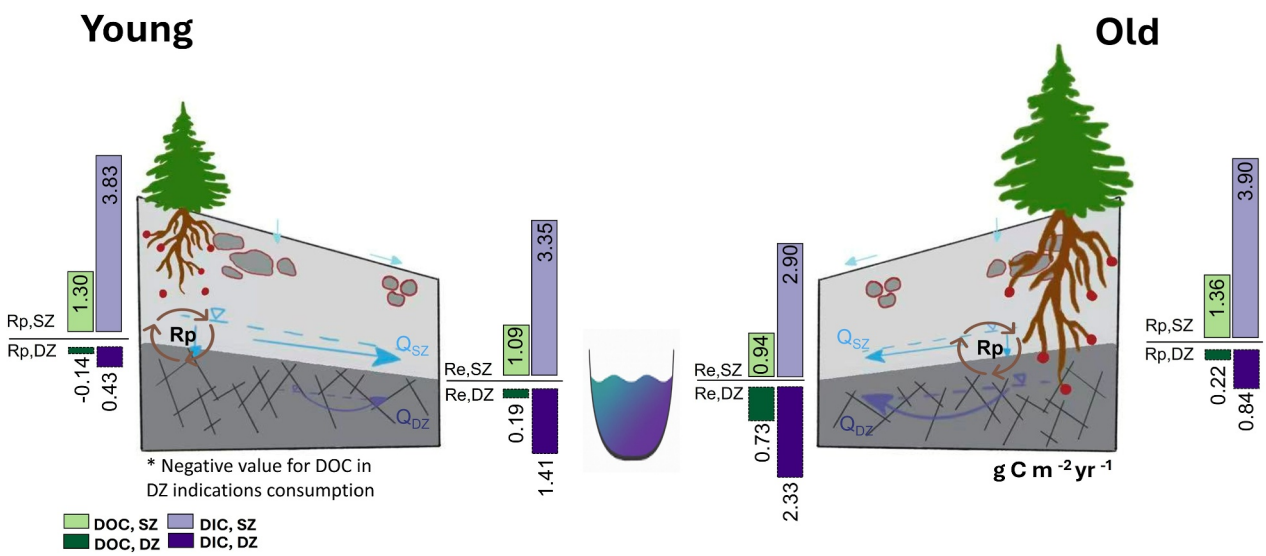

Figure 7. Summary of dissolved carbon production (R_p; g C m^{-2} yr^{-1}) and export (R_e; g C m^{-2} yr^{-1}) in the shallow (SZ) and deep zones (DZ) of the modeled young (WS01) and old (WS02) forest catchments. Compared to the young forest, the old forest exhibits greater DOC and DIC production and export from the deep zone, reflecting enhanced deep respiration and hydrological connectivity that sustain higher dissolved carbon fluxes to the stream.

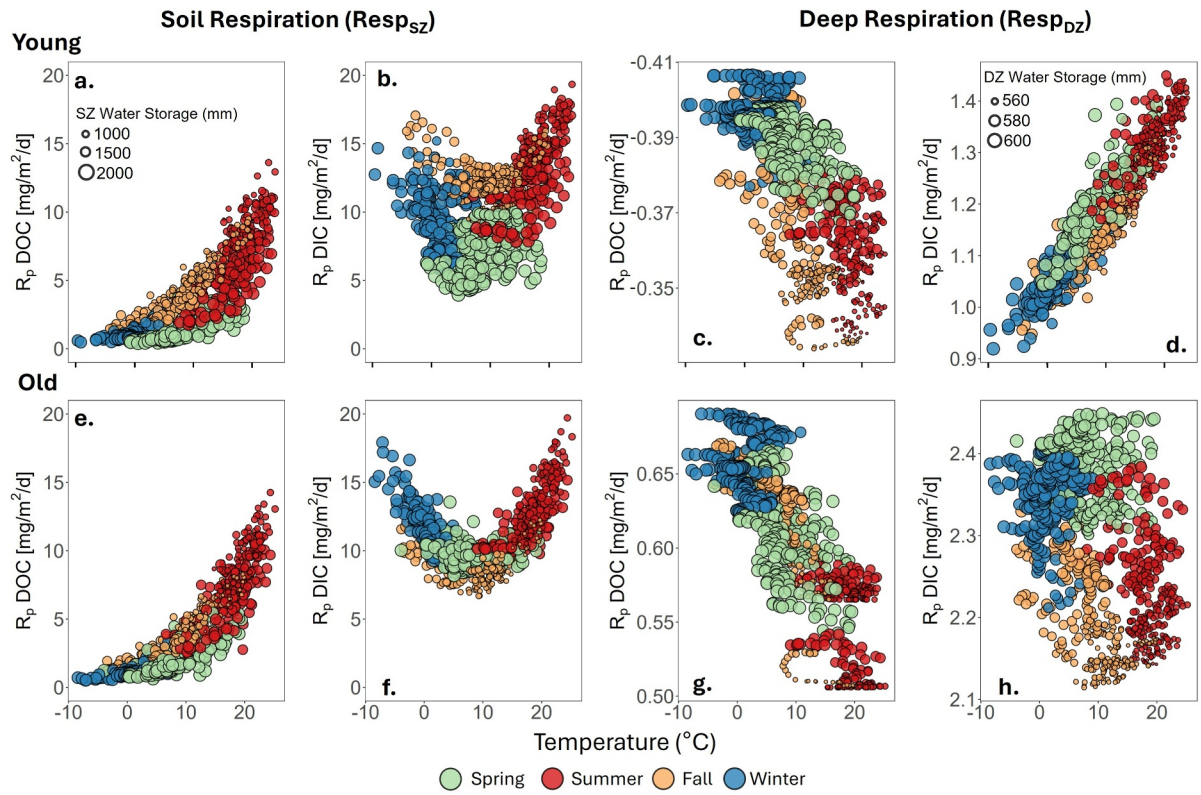

Figure 8. Modeled soil respiration ($Resp_{SZ}$) in the shallow zone (SZ) and deep respiration ($Resp_{DZ}$) in the deep zone (DZ) for DOC and DIC production, shown as functions of air temperature and water storage for the young (top) and old forest (bottom). DOC production in the SZ is primarily temperature-driven, peaking during summer. In DZ, DOC production is more strongly influenced by water storage. DIC production in the SZ exhibits dual dependence on temperature and water storage, resulting in a double peak with higher rates in summer and winter. In DZ, DIC production in the young increases with temperature, while in the old forest, it is more strongly driven by water storage.

9.1 ± 6.4 mg m^{-2} d^{-1}. Mean $R_{e,\,DIC}$ was 14.3 ± 15.4 mg m^{-2} d^{-1}, with 8.0 ± 13.3 mg m^{-2} d^{-1} from the shallow zone and a comparatively large 6.4 ± 3.7 mg m^{-2} d^{-1} from the deep zone (Figure 6h, purple). Winter peaks reached 27.7 ± 18.7 mg m^{-2} d^{-1}.

3.5. Drivers of Dissolved Carbon Production and Export

Soil respiration in the shallow zone drove DOC production primarily through daily temperature dependence, following a clear exponential seasonal pattern across both forests (Figures 8a and 8e). Rates peaked during summers with elevated temperatures and declined sharply as temperatures dropped and water storage increased during the transition to the cool, wet seasons. In the deep zone, DOC reaction rates exhibited contrasting behaviors between the two forests. In the young forest, DOC from the shallow zone was further transformed to DIC in the deep zone, whereas in the old forest, additional DOC was produced. In both forests, deep respiration rates followed water storage, peaking during the wet winter months when water storage was at its maximum and declining as storage decreased (Figures 8c and 8g).

The rates for DIC production in the shallow zone showed a distinctive V-shaped seasonal pattern, with a minimum at an intermediate temperature around 10°C (Figures 8b and 8f). Peak production occurred during summer months, coinciding with maximum air temperatures, and again during the winter months, corresponding to the lowest temperatures but maximum water storage. This pattern is consistent with their rate dependence on soil moisture in Equation 5. DIC production in the deep zone was controlled by different drivers between the forests. In the young forest, DIC production rates increased with air temperature and peaked during the summer months (Figure 8d). Conversely, in the old forest, DIC production rates in the deep zone were primarily water storage driven, peaking during the wet spring and winter (Figure 8h).

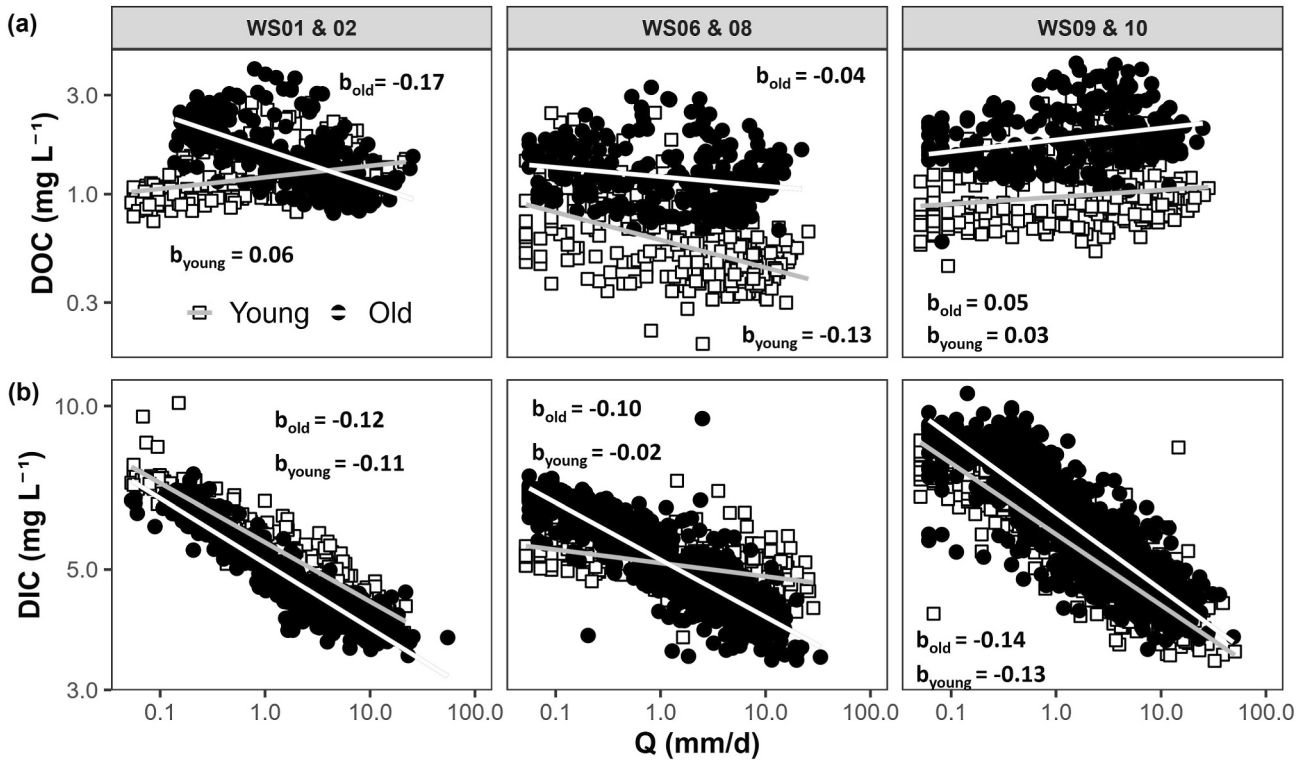

Figure 9. Observed concentration discharge (CQ) relationships for (a) DOC and (b) DIC across three young-old forest pairs. Black circles and white regression lines represent the old forests, while open squares and gray regression lines represent the young forests. Within each panel, the CQ slopes (b) for the corresponding young and old forests are shown. DOC CQ relationship *b* slopes (in $C = aQ^b$) vary across different pairs, whereas DIC consistently shows dilution behavior, with stronger dilution patterns across all old forests.

3.6. Numerical Experiments and Diverse Carbon Dynamics Across Young and Old Forests

In all three pairs of young and old forests, dissolved carbon concentrations differ in old and young forests. Mean stream DOC concentrations were consistently higher in old forests (1.61 ± 0.65 mg L^{-1}) compared to young forests (0.98 ± 0.48 mg L^{-1}). Similarly, mean stream DIC concentrations are 5.50 ± 1.33 mg L^{-1} and 5.49 ± 1.16 mg L^{-1} in old and young forests, respectively. In all streams, DIC concentrations are higher than DOC concentrations, a common observation in rivers and streams. For CQ relationships, DIC exhibited consistent dilution patterns in all catchments, but DOC showed diverse patterns across pairs, not necessarily aligning with forest age (Figure 9; Table S7 in Supporting Information S1 for regression statistics). Although WS01 (young) and WS02 (old) showed contrasting patterns, WS06 (young) and WS08 (old) exhibited dilution and chemostatic, and WS09 (old) and WS10 (young) displayed weak flushing and chemostatic behavior. Note that all these *b* values are relatively close to zero values, likely a result of composite sampling that masked some of the temporal variations in concentrations.

To understand processes and variables that lead to the differences in concentrations and CQ patterns of dissolved carbon, we conducted numerical thought experiments using the calibrated WS01 model as a baseline configuration (Detailed design in Section 2.9). The five variables have distinct impacts on depth profiles, concentration levels, and CQ patterns of DOC (Figure 10). Increasing Q_{DZ}% (Figure 10a), the proportion of water flow routed through the deep zone, dampened DOC CQ variability with minimal changes in CQ slope values ($b = 0.02-0.05$). This is because concentrations in the deeper zone generally have much lower variation. Different DOC reaction types in deep zone controlled the CQ slope direction (Figure 10b). With deep consumption (–DOC), deep DOC concentrations were lower than those in the shallow zone, producing a flushing CQ pattern ($b = 0.09$). In contrast, when no DOC reactions occurred in the deep zone (0DOC), DOC concentrations were similar across different depths, resulting in a near chemostatic to weak dilution pattern ($b = -0.05$). When DOC production (+DOC) occurred in the deep zone, DOC concentrations exceeded those in the shallow zone, yielding a strong dilution CQ pattern ($b = -0.20$).

10.1029/2025WR040838

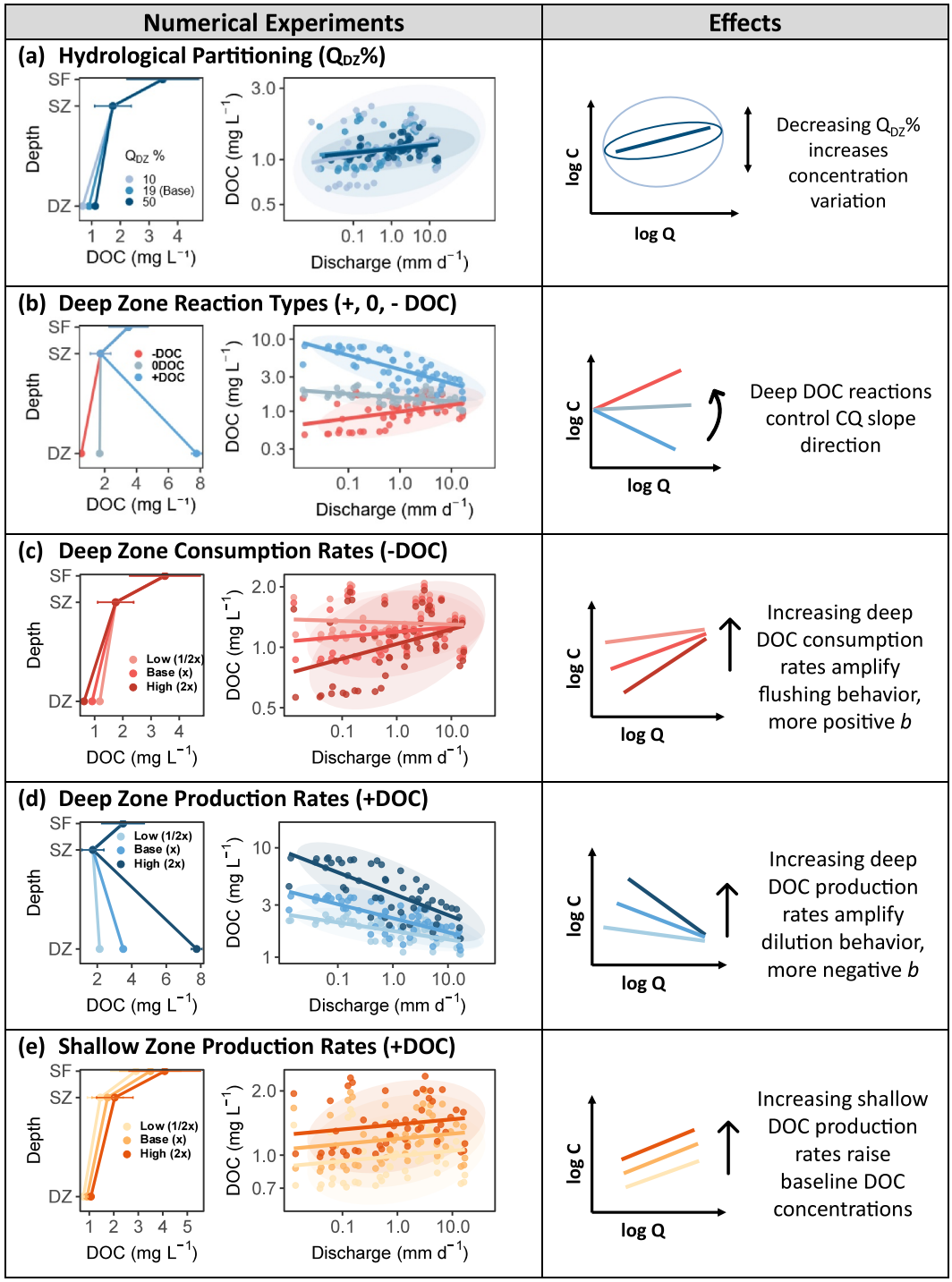

Figure 10. Summary of numerical experiments and schematic overview illustrating the influence of five variables (hydrological flow partitioning, reaction types, and reaction rates across shallow and deep zones) on the depth profiles and CQ patterns, using DOC as an example. (a) Increasing the proportion of deep zone flow (Q_{DZ}%) reduces the concentration scatter and variability within the CQ space. (b) Deep zone DOC production versus consumption processes controls the direction of depth profiles and CQ slopes. (c) Increasing deep DOC consumption rates amplifies concentration gradients in depth profiles and flushing behavior. (d) Increasing deep DOC production rates amplifies concentration gradients in depth profiles and dilution behavior. (e) Increasing shallow zone DOC production rates raise baseline DOC concentration in depth profile and CQ intercept. The interplay between hydrological flow partitioning and subsurface processes governs the direction and magnitude of DOC CQ relationships in forested catchments.

The rates of DOC production (+DOC) or consumption (–DOC) determines the intensity of the resulting CQ patterns. When deep DOC consumption rates are high, DOC concentrations at depth decrease, leading to more flushing behavior (Figure 10c). Lower deep consumption rates allow DOC to accumulate in the deep zone, reducing vertical concentration contrasts and yielding a near-chemostatic response. Here, the baseline scenario produced a slope b of 0.02; increasing the deep consumption rate strengthened flushing (b = 0.07), whereas decreasing it produced an almost chemostatic pattern (b = −0.01). Conversely, when DOC is produced in the deep zone (+DOC) (Figure 10d), higher production rates amplified dilution behavior by increasing deep zone DOC concentrations, while lower rates weakened the dilution response. The baseline deep production scenario produced a CQ slope of b = –0.13; increasing the production rate enhanced dilution (b = –0.2), while decreasing the rate reduced it toward chemostatic conditions (b = –0.08). Finally, DOC production in the shallow zone primarily controlled baseline DOC concentrations rather than CQ slope (Figure 10e). Increasing shallow production elevated DOC concentrations throughout the profile but did not substantially change the export pattern, which remained weakly flushing ($b \approx 0.02$). This reflects that most dissolved carbon originates from shallow soils, which largely set the baseline DOC levels exported to streams.

4. Discussion

4.1. Important but Insufficient Role of Forest age in Shaping DOC Export Patterns

Distinct CQ export patterns between WS01 and WS02 reflect the dominant influence of forest age. In these two forests, stream chemistry and subsurface data are consistent with our hypothesis of contrasting DOC export patterns arising from distinct subsurface structures in young and old forests; the old forest (WS02) show a dilution pattern, whereas the young (WS01) showed a flushing behavior. In both forests, model results indicate that DOC is predominantly produced in shallow soil zones, but the nature of carbon reactions differs in the deeper zone. In the old forest, deeper and denser fine roots (Figure 5b) likely promote root exudation and carbon decomposition at depth, resulting in contrasting depth profiles of DOC that translate into divergent CQ behaviors (Figures 4 and 5). This pattern, together with root data, aligns with the Shallow and Deep Hypothesis, which links source depth and flow paths to solute export dynamics (Stewart, Shanley, et al., 2022; Zhi & Li, 2020). The rarity of DOC dilution in natural streams (e.g., Botter et al., 2020; Godsey et al., 2019; Kincaid et al., 2024) underscores the dominant role of forest age in shaping CQ export patterns.

While these contrasts highlight the importance of forest age, it cannot explain diverse DOC patterns across other young and old forests. In WS06 and WS08, both streams show unusual dilution patterns, whereas WS09 and WS10 show patterns that range from flushing to chemostatic (Figure 9). Although each pair experiences similar climate and elevation internally, elevation and geology differ among pairs (Johnson et al., 2021). The upper elevation pair (WS06&WS08; ∼900 m) receives greater precipitation and a higher snow fraction than the lower elevation pairs (WS01&WS02 and WS09&WS10; ∼400 m). The lower elevation pairs are underlain by highly weathered Oligocene tuffs and breccias, whereas the upper elevation pair is underlain by Miocene andesitic basalt lava flow. These contrasting geologic formations influence soil development and permeability, with finer-textured soils typically forming over the older tuffs and breccias and more loamy, well-drained soils associated with the basaltic units (Swanson, 1975). Such differences likely influence how water and dissolved carbon move through the subsurface. In the old forest WS09, although the climate, elevation, and geology are similar to WS02, forest age appears to not be as influential as that in WS02, leading to the more commonly observed flushing pattern. Indeed, across HJA, emergent patterns in subsurface water storage and connectivity have been identified as key regulators of stream chemistry (Ortega et al., 2025a, Ortega, Bush, et al., 2025), reinforcing that local subsurface structure must be considered when interpreting CQ relationships.

Numerical thought experiments further support the idea that biogeochemical reactions and concentration gradient over depth control CQ patterns (Figure 10). A general principle emerged from these experiments is that reaction types, whether consumption or production at depth, determine the directionality (positive or negative b values) of export patterns, whereas reaction rates regulate the strength or magnitude of export patterns. Reaction rates that minimize shallow-vs-deep concentration gradients lead to chemostatic patterns, whereas those amplify concentration gradients over depth strengthen export patterns with higher absolute b values.

Results here resonate with broad theory of the Shallow and Deep Hypothesis, which posits that flow paths transport solutes with distinct chemical signatures depending on their source depth (Stewart, Shanley, et al., 2022; Zhi & Li, 2020). Hydrologic partitioning is controlled by subsurface physical structure (porosity, permeability,

vertical connectivity), which is itself shaped by vegetation, soils, and bedrock (Ameli et al., 2017; Sullivan et al., 2022; Tetzlaff et al., 2009, 2014; Xiao et al., 2021). Meanwhile, biogeochemical reaction rates (DOC production vs. consumption) depend on organic matter distribution, mineral reactivity, root inputs, and microbial communities (Riebe et al., 2017; Sullivan et al., 2022; Wen et al., 2022; Wymore et al., 2017). At continental scales, Stewart and Li (2025), using data from hundreds of minimally disturbed U.S. catchments (CAMELS-CHEM), demonstrated that vertical concentration gradients (shallow vs. deep) primarily dictate the direction of solute CQ slopes, while relative contributions of shallow versus deep flow control concentration variability. Findings here highlight the importance of deep subsurface processes including root-derived inputs and microbial activities in sustaining DOC availability and shaping export dynamics. Collectively, these insights suggest that forest age is a useful but insufficient predictor of DOC export behavior, with subsurface structure and biogeochemical mechanism serving as more fundamental controls.

4.2. Higher Contribution of Deep Groundwater Flow Indicates Higher Vertical Connectivity in Old Forests

Although WS01 (young) and WS02 (old) share similar climate, elevation, and geology, their hydrology differs substantially. Annual streamflow in the young forest was on average 18.5% lower than in the old forest, and this difference reached up to 45% lower in the summer. Streamflow deficits in young forests, particularly during low-flow periods, are consistent with patterns in other regenerating plantations (Crampe et al., 2021; Dye, 1996; Garcia et al., 2018; Segura et al., 2020). These deficits are commonly attributed to their higher transpiration, where rapid growth and dense foliage increase water use and limits water availability (Feikema et al., 2010; Perry & Jones, 2017; Tuswa et al., 2019).

Model results here suggest, however, that vegetation water use alone may not fully explain these contrasts. Modeled actual evapotranspiration (AET) was comparable between the two forests ($1{,}280 \pm 85$ mm yr^{-1} in WS01 and $1{,}260 \pm 105$ mm yr^{-1} in WS02; Table S5 in Supporting Information S1), indicating similar overall water balance at the catchment scale. Although HBV may overestimate actual evapotranspiration due to the close water balance assumption, the relative similarity between the two forests remains informative. While this modeled similarity does not preclude higher tree-level transpiration in the young forest (Moore et al., 2004), it highlights that other processes, particularly those related to subsurface water movement and storage, likely also contribute to the observed streamflow differences at the catchment scale.

Model simulations indicate that ~30% of streamflow originates from deep groundwater flow (Q_{DZ}) in the old forest, compared to about 20% in the young forest, consistent with previous estimates for these catchments (Waichler et al., 2005). In the old forest, deeper and denser fine roots (Figure 5b) have been commonly observed in old forests (Hertel et al., 2003; Jagodzinski et al., 2016; Sarai et al., 2022; Yanai et al., 2006), which likely enhance macropore development and vertical connectivity, facilitating greater infiltration and sustained baseflow (Bauhus, 2009; Sullivan et al., 2022). In contrast, the less dense root systems in the young forest may not recharge as much water to the deep zone. Direct measurement of such subsurface processes remains challenging (Brantley et al., 2017; Brooks et al., 2015; McDonnell et al., 2018; Sullivan et al., 2024), yet these structural differences likely control how water partitions between rapid, shallow flow and slower, deeper flows, ultimately governing the magnitude, timing, and persistence of streamflow (Xiao et al., 2019).

4.3. Higher Dissolved Carbon Indicates Higher Carbon Production Versus Export in Old Forests

Results here show that all streams draining old forests have higher concentrations of dissolved carbon (both organic and inorganic) than those draining young forests. This pattern aligns with findings in these same sites (Hood et al., 2006; Lee & Lajtha, 2016) and from other ecosystems (Cawley et al., 2014; Fegel et al., 2021). For example, Fegel et al. (2021) reported that old subalpine forests exported roughly five times more DOC than second-growth pine forests regenerating from clearcutting, with DOC in the old also more aromatic and enriched in plant-derived organic acids. At Hubbard Brook Experimental Forest, Cawley et al. (2014) similarly observed higher DOC concentrations in streams draining old reference forests compared to their clearcut counterparts. They further showed that DOC from clearcut forests carried fluorescence signatures enriched in microbial sources, whereas old forests exported DOC with greater aromatic compounds, which is consistent with deeper subsurface carbon dynamics that sustain DOC availability in old forests. Broadly, many cations and nitrate exhibit systematically higher concentrations in streams draining old versus young forest in, for example, Hubbard Brook

(Cawley et al., 2014; Vitousek & Reiners, 1975). For nutrients, such differences have been attributed to higher nutrient demands in young forests, leading to more "tightly" cycled and therefore lower export (Vitousek & Reiners, 1975).

Higher concentrations often reflect higher rates of "production" or input compared to export and output (Li et al., 2022), which may suggest that higher stream carbon in old forests arise from higher carbon "production" in old compared to young forests. At the ground surface, old forests tend to accumulate more woody debris and organic-rich litter layers, and mean annual DOC flux in HJA have been shown to increase with forest floor wood biomass (Lajtha & Jones, 2018). Such pools may continuously provide leachable DOC, particularly during rainfall events. In addition, belowground carbon allocation and root–soil interactions likely play an important role. Old forests have been reported to have greater fine roots compared to younger forests (Hertel et al., 2003; Jagodzinski et al., 2016; Sarai et al., 2022; Yanai et al., 2006). Subsurface data from WS01 and WS02 support this interpretation, as the old forest exhibited greater fine root biomass at deeper depths compared to the young forest (Figure 5b). These fine roots are key conduits for carbon inputs into soil via root exudates and downward transport of DOC (Rumpel & Kögel-Knabner, 2011). Greater fine roots can enhance respiration (Trumbore et al., 2006), possibly elevating concentrations of dissolved carbon, especially DIC. In addition, root exudates of low-molecular-weight can feed microbial communities, stimulate decomposition of soil organic matter and release CO_2 or labile DOC (He et al., 2020; Moore et al., 2020). Together, these surface and subsurface mechanisms likely increase the availability and mobility of dissolved carbon in old forests, potentially suggesting that old forests play a more important role in land-to-river carbon transport and dissolved carbon cycling.

4.4. Consistent Dilution Patterns Indicate Deep Respiration at Depth

In all streams, DIC exhibited a dilution export pattern, consistent with near-universal dilution patterns of DIC and alkalinity observed across US and globe (Godsey et al., 2019; Marx et al., 2017; Stewart & Li, 2025; Stewart, Zhi, et al., 2022). This pattern reflects key biogeochemical structure and reactions driving subsurface DIC gradients that are consistent with the Shallow and Deep Hypothesis (Stewart, Shanley, et al., 2022; Zhi & Li, 2020). HJA contains negligible carbonate materials (Swanson, 1975) such that the dominant DIC source is respiration. Although most respiration occurs in shallow soil, CO_2 losses to the atmosphere from upper soil layers reduce DIC availability in shallow zones (Keller, 2019), leading to typically lower concentrations in shallow soil and higher concentrations in the deeper subsurface (Carbone et al., 2023; Stolze et al., 2024; Tune et al., 2020). In addition, DOC and DIC in shallow soil can be transported downward with water, where DOC may undergo further respiration to become CO_2 and DIC, therefore adding DIC at depth. As stream water derives more from deeper groundwater as base flow and shallow soil water at high flow, stream DIC almost universally shows dilution patterns with high DIC at low flow and low DIC at high flow (Stewart & Li, 2025). Deep respiration is essential in shaping such dilution patterns: without deep respiration, CQ patterns exhibit chemostatic behaviors with very similar concentrations at low and high flow, contrasting patterns observed in global stream DIC data (Kerins et al., 2024; Stewart & Li, 2025). Deep respiration has been directly observed at depths tens of meters below-ground (Tune et al., 2020). More recently, majority of the riverine CO_2 emitted to atmosphere (~60%) have been shown to be millennial or older (Dean et al., 2025; Li, 2025), further corroborating the widespread occurrence of deep respiration.

Model results indicate that deep respiration produces nearly twice as much DIC in the old forest compared to the young forest. Additionally, the old forest exports approximately 65% more DIC from the deep zone compared to the young forest. This higher export is facilitated by the old forest's greater groundwater contribution to streamflow. Although all forests exhibit similar dilution patterns for DIC, the *b* slope values are more negative in old forests, pointing to stronger signatures of deep respiration in old forests. Long-term observations report rising groundwater DIC concentrations, attributed to partial recovery from atmospheric sulfate deposition, shifting weathering regimes, and increased soil respiration driven by forest regrowth and productivity (Klaus, 2023). This suggests that dissolved carbon dynamics will continue to evolve and can serve as signals of changing subsurface structure and processes, particularly as forest landscapes continue to transition under changing management and environmental conditions.

4.5. Model Limitations

As a spatially implicit model, BioRT-HBV represents average, effective catchment-scale dynamics and does not account for spatial variability across landscape positions. This simplification is necessary given the lack of detailed spatial data to support more complex parameterizations and to reduce issues of equifinality (Li, 2019). It also means the model cannot distinguish between distinct zones such as riparian areas and hillslopes, which play different roles in carbon cycling (Dick et al., 2015; Findlay et al., 2001). At HJA, fast-growing deciduous vegetation typically dominates riparian zones and the understory of upland areas, whereas Douglas fir remains the dominant overstory species across most of the landscape (Johnson et al., 2021). Such differences in tree composition can influence organic matter inputs and subsurface carbon dynamics between hillslopes and riparian areas but cannot be explicitly represented in our lumped model structure. The hyporheic zone is not explicitly represented, even though it can be important in forested headwater systems (Corson-Rikert et al., 2016). The model also does not include internal ecosystem changes associated with vegetation succession, soil development, or long-term biogeochemical shifts. Even when forced with multi-decadal inputs, its parameters remain fixed and cannot evolve with ecosystem state. Thus, it is beyond the scope of this study to investigate long-term DOC changes, such as the declines observed across 11 years of data record in WS01 (Rodríguez-Cardona et al., 2022), or potential future shifts expected under warmer and drier conditions driven by climate change in the Pacific Northwest (Campbell et al., 2022).

In addition, soil respiration is represented as a lumped reaction with a generic soil organic carbon pool. This reaction simultaneously produces DOC and CO_2(aq), the latter contributing to the DIC pool. However, the model does not simulate vertical CO_2 effluxes, a major component of forest carbon budget (Argerich et al., 2016; Campbell & Law, 2005; Jassal et al., 2004). As a result, the estimated soil respiration rates reflect only the portion that contributes to dissolved carbon production. The model also does not account for in-stream carbon processing, such as transformation, uptake, or outgassing, even though they can be important in carbon cycling (Hotchkiss et al., 2015).

5. Conclusion

This study demonstrates distinct subsurface hydrological and biogeochemical processes that jointly regulate dissolved carbon production and export in forests of different ages. Using the model BioRT-HBV, we examined DOC and DIC dynamics in paired catchments at the H.J. Andrews Experimental Forest. Model simulations and field observations together reveal that dissolved carbon cycling is strongly depth-dependent and controlled by both subsurface flow partitioning and reaction processes. Although both forests produce most dissolved carbon in the shallow subsurface, the magnitude and vertical distribution of production differ substantially. In the young forest, DOC production is concentrated near the surface, and the deep zone acts as a net sink, producing a flushing CQ pattern. In the old forest, deeper and denser roots sustain DOC production at depth, maintaining high deep zone DOC and DIC concentrations and producing dilution CQ behavior. These contrasting relationships highlight how rooting depth and subsurface connectivity regulate the balance between carbon transformation and transport. Extending beyond a single pair, other young old pairs show diverse DOC export behaviors that cannot be explained by forest age alone, reflecting the influence of local catchment context on hydrologic connectivity and carbon reactivity. Collectively, these results suggest that differences in subsurface structure, rather than forest age alone, are key to explaining variability in dissolved carbon export from forested watersheds. As forests continue to recover from historical deforestation and experience shifts in species composition, management, and climate, accounting for subsurface processes, especially those linked to rooting depth, vertical connectivity, and geological setting, will be essential for predicting long-term carbon cycling in forested landscapes.

Conflict of Interest

The authors declare no conflicts of interest relevant to this study.

Data Availability Statement

Hydrometeorology and aqueous chemistry data from the H.J. Andrews Experimental Forest used for this study are available in the following references (Daly et al., 2019; Johnson et al., 2024; Johnson & Fredriksen, 2019a, 2019b). The source code and example files for BioRT-HBV are available at Sadayappan et al. (2024b). Model input and output files used for this study are available at Liu et al. (2025).

Acknowledgments

This research was supported by the National Science Foundation (Grants EAR-2121621; EAR-2121694 [PLS]; 2034232 [PLS]; 2121639 [SAB]; 2121760 [HA/DRH]; 1943573 [CS]; 2424997 [CS]). Additional support was provided by the USDA National Institute of Food and Agriculture through the Signals in the Soil Grants (2021-67019-34341 [HA/DRH]; 2021-67019-34338 [SAB]; 2021-67019-34340 [AF]). Any opinions, findings, and conclusions or recommendations expressed in this material are those of the authors and do not necessarily reflect the views of the National Science Foundation or the USDA. Streamflow and climate data were provided by the H.J. Andrews Experimental Forest and Long-Term Ecological Research (LTER) program, administered cooperatively by Oregon State University, the USDA Forest Service Pacific Northwest Research Station, and the Willamette National Forest. This material is based upon work supported by the National Science Foundation under the Grant LTER8 DEB-2025755. We thank Dr. Kamini Singh, Dr. Jesse Nippert, and Dr. Sherri Johnson for their valuable feedback and suggestions on earlier drafts of this manuscript.

References

Abril, G., Bouillon, S., Darchambeau, F., Teodoru, C. R., Marwick, T. R., Tamooh, F., et al. (2014). Technical note: Large overestimation of pCO2 calculated from pH and alkalinity in acidic, organic-rich freshwaters. *Biogeochemistry: Rivers & Streams*. https://doi.org/10.5194/bgd-11-11701-2014

Ågren, A., Buffam, I., Jansson, M., & Laudon, H. (2007). Importance of seasonality and small streams for the landscape regulation of dissolved organic carbon export. *Journal of Geophysical Research*, *112*(G3). https://doi.org/10.1029/2006JG000381

Ameli, A. A., Beven, K., Erlandsson, M., Creed, I. F., McDonnell, J. J., & Bishop, K. (2017). Primary weathering rates, water transit times, and concentration-discharge relations: A theoretical analysis for the critical zone. *Water Resources Research*, *53*(1), 942–960. https://doi.org/10.1002/2016WR019448

Argerich, A., Haggerty, R., Johnson, S. L., Wondzell, S. M., Dosch, N., Corson-Rikert, H., et al. (2016). Comprehensive multiyear carbon budget of a temperate headwater stream. *Journal of Geophysical Research: Biogeosciences*, *121*(5), 1306–1315. https://doi.org/10.1002/2015JG003050

Bauhus, J. (2009). Rooting patterns of old-growth forests: Is aboveground structural and functional diversity mirrored belowground? In C. Wirth, G. Gleixner, & M. Heimann (Eds.), *Old-Growth forests: Function, fate and value* (pp. 211–229). Springer. https://doi.org/10.1007/978-3-540-92706-8_10

Beck, H. E., van Dijk, A. I. J. M., de Roo, A., Miralles, D. G., McVicar, T. R., Schellekens, J., & Bruijnzeel, L. A. (2016). Global-scale regionalization of hydrologic model parameters. *Water Resources Research*, *52*(5), 3599–3622. https://doi.org/10.1002/2015WR018247

Bergström, S. (1976). Development and application of a conceptual runoff model for Scandinavian catchments. https://urn.kb.se/resolve?urn=urn:nbn:se:smhi:diva-5738

Billings, S. A., Hirmas, D., Sullivan, P. L., Lehmeier, C. A., Bagchi, S., Min, K., et al. (2018). Loss of deep roots limits biogenic agents of soil development that are only partially restored by decades of forest regeneration. *Elementa: Science of the Anthropocene*, *6*, 34. https://doi.org/10.1525/elementa.287

Bingham, B. B., Jr., & Sawyer, J. O. (2022). Canopy structure and tree condition of young, mature, and old-growth Douglas-fir/hardwood forests. In R. R. Harris & D. E. Erman (Eds.), *Proceedings of the Symposium on Biodiversity of Northwestern California; 1991 October 28-30* (pp. 141–149). University of California. Retrieved from https://research.fs.usda.gov/treesearch/3474

Blanchet, C. C., Arzel, C., Davranche, A., Kahilainen, K. K., Secondi, J., Taipale, S., et al. (2022). Ecology and extent of freshwater browning—What we know and what should be studied next in the context of global change. *Science of the Total Environment*, *812*, 152420. https://doi.org/10.1016/j.scitotenv.2021.152420

Botter, M., Li, L., Hartmann, J., Burlando, P., & Fatichi, S. (2020). Depth of solute generation is a dominant control on concentration-discharge relations. *Water Resources Research*, *56*(8), e2019WR026695. https://doi.org/10.1029/2019WR026695

Brantley, S. L., Eissenstat, D. M., Marshall, J. A., Godsey, S. E., Balogh-Brunstad, Z., Karwan, D. L., et al. (2017). Reviews and syntheses: On the roles trees play in building and plumbing the critical zone. *Biogeosciences*, *14*(22), 5115–5142. https://doi.org/10.5194/bg-14-5115-2017

Brooks, P. D., Chorover, J., Fan, Y., Godsey, S. E., Maxwell, R. M., McNamara, J. P., & Tague, C. (2015). Hydrological partitioning in the critical zone: Recent advances and opportunities for developing transferable understanding of water cycle dynamics. *Water Resources Research*, *51*(9), 6973–6987. https://doi.org/10.1002/2015WR017039

Campbell, J. L., Driscoll, C. T., Jones, J. A., Boose, E. R., Dugan, H. A., Groffman, P. M., et al. (2022). Forest and freshwater ecosystem responses to climate change and variability at US LTER sites. *BioScience*, *72*(9), 851–870. https://doi.org/10.1093/biosci/biab124

Campbell, J. L., & Law, B. E. (2005). Forest soil respiration across three climatically distinct chronosequences in Oregon. *Biogeochemistry*, *73*(1), 109–125. https://doi.org/10.1007/s10533-004-5165-9

Carbone, M. S., Richardson, A. D., Barr, B., Berkelhammer, M., Boot, C. M., Simonpietri, A., & Still, C. J. (2023). Interannual precipitation controls on soil CO2 fluxes in high elevation conifer and aspen forests. *Environmental Research Letters*, *18*(12), 124009. https://doi.org/10.1088/1748-9326/ad07b5

Carle, J., & Vuorinen, P. (2002). Status and trends in global Forest plantation development. *Forest Products Journal*, *52*(7).

Cawley, K. M., Campbell, J., Zwilling, M., & Jaffé, R. (2014). Evaluation of forest disturbance legacy effects on dissolved organic matter characteristics in streams at the Hubbard Brook experimental Forest, New Hampshire. *Aquatic Sciences*, *76*(4), 611–622. https://doi.org/10.1007/s00027-014-0358-3

Corson-Rikert, H. A., Wondzell, S. M., Haggerty, R., & Santelmann, M. V. (2016). Carbon dynamics in the hyporheic zone of a headwater mountain stream in the Cascade Mountains, Oregon. *Water Resources Research*, *52*(10), 7556–7576. https://doi.org/10.1002/2016WR019303

Crampe, E. A., Segura, C., & Jones, J. A. (2021). Fifty years of runoff response to conversion of old-growth forest to planted forest in the H. J. Andrews Forest, Oregon, USA. *Hydrological Processes*, *35*(5), e14168. https://doi.org/10.1002/hyp.14168

Curtis, P. G., Slay, C. M., Harris, N. L., Tyukavina, A., & Hansen, M. C. (2018). Classifying drivers of global forest loss. *Science*, *361*(6407), 1108–1111. https://doi.org/10.1126/science.aau3445

Daly, C., Schulze, M., & McKee, W. (2019). *Meteorological data from benchmark stations at the HJ Andrews Experimental Forest, 1957 to present. Long-Term Ecological Research*. Forest Science Data Bank. https://doi.org/10.6073/pasta/c021a2ebf1f91adf0ba3b5e53189c84f

Davidson, E. A., & Janssens, I. A. (2006). Temperature sensitivity of soil carbon decomposition and feedbacks to climate change. *Nature*, *440*(7081), 165–173. https://doi.org/10.1038/nature04514

Davidson, E. C. A., Belk, E., & Boone, R. D. (1998). Soil water content and temperature as independent or confounded factors controlling soil respiration in a temperate mixed hardwood forest. *Global Change Biology*, *4*(2), 217–227. https://doi.org/10.1046/j.1365-2486.1998.00128.x

Dean, J. F., Coxon, G., Zheng, Y., Bishop, J., Garnett, M. H., Bastviken, D., et al. (2025). Old carbon routed from land to the atmosphere by global river systems. *Nature*, *642*(8066), 105–111. https://doi.org/10.1038/s41586-025-09023-w

Dick, J. J., Tetzlaff, D., Birkel, C., & Soulsby, C. (2015). Modelling landscape controls on dissolved organic carbon sources and fluxes to streams. *Biogeochemistry*, *122*(2), 361–374. https://doi.org/10.1007/s10533-014-0046-3

Du, Z., Yu, L., Yang, J., Xu, Y., Chen, B., Peng, S., et al. (2022). A global map of planting years of plantations. *Scientific Data*, *9*(1), 141. https://doi.org/10.1038/s41597-022-01260-2

Dudley, N., & Stolton, S. (2003). *Running pure: The importance of forest protected areas to drinking water*. World Bank / WWF Alliance for Forest Conservation and Sustainable Use. Retrieved from https://bvearmb.do/handle/123456789/3913

Dye, P. J. (1996). Climate, forest and streamflow relationships in South African afforested catchments. *Commonwealth Forestry Review*, *75*(1), 31–38.

Dyrness, C. T. (1973). Early stages of plant succession following logging and burning in the Western cascades of Oregon. *Ecology*, *54*(1), 57–69. https://doi.org/10.2307/1934374

Fang, C., & Moncrieff, J. B. (2005). The variation of soil microbial respiration with depth in relation to soil carbon composition. *Plant and Soil*, *268*(1), 243–253. https://doi.org/10.1007/s11104-004-0278-4

Fegel, T. S., Boot, C. M., Covino, T. P., Elder, K., Hall, E. K., Starr, B., et al. (2021). Amount and reactivity of dissolved organic matter export are affected by land cover change from old-growth to second-growth forests in headwater ecosystems. *Hydrological Processes*, *35*(8), e14343. https://doi.org/10.1002/hyp.14343

Feikema, P. M., Morris, J. D., & Connell, L. D. (2010). The water balance and water sources of a Eucalyptus plantation over shallow saline groundwater. *Plant and Soil*, *332*(1), 429–449. https://doi.org/10.1007/s11104-010-0309-2

Findlay, S., Quinn, J. M., Hickey, C. W., Burrell, G., & Downes, M. (2001). Effects of land use and riparian flowpath on delivery of dissolved organic carbon to streams. *Limnology & Oceanography*, *46*(2), 345–355. https://doi.org/10.4319/lo.2001.46.2.0345

Fontaine, S., Barot, S., Barré, P., Bdioui, N., Mary, B., & Rumpel, C. (2007). Stability of organic carbon in deep soil layers controlled by fresh carbon supply. *Nature*, *450*(7167), 277–280. https://doi.org/10.1038/nature06275

Fredriksen, R. L. (1969). A battery powered proportional stream water sampler. *Water Resources Research*, *5*(6), 1410–1413. https://doi.org/10.1029/WR005i006p01410

Fredriksen, R. L. (2019). Stream chemistry concentrations and fluxes using proportional sampling in the Andrews Experimental forest, 1968 to present [Dataset]. *Environmental Data Initiative*. https://doi.org/10.6073/PASTA/BB935444378D112D9189556FD22A441D

Frisbee, M. D., Wilson, J. L., Gomez-Velez, J. D., Phillips, F. M., & Campbell, A. R. (2013). Are we missing the tail (and the tale) of residence time distributions in watersheds? *Geophysical Research Letters*, *40*(17), 4633–4637. https://doi.org/10.1002/grl.50895

Garcia, L. G., Salemi, L. F., Lima, W., de, P., & Ferraz, S. F. B. (2018). Hydrological effects of forest plantation clear-cut on water availability: Consequences for downstream water users. *Journal of Hydrology: Regional Studies*, *19*, 17–24. https://doi.org/10.1016/j.ejrh.2018.06.007

Godsey, S. E., Hartmann, J., & Kirchner, J. W. (2019). Catchment chemostasis revisited: Water quality responds differently to variations in weather and climate. *Hydrological Processes*, *33*(24), 3056–3069. https://doi.org/10.1002/hyp.13554

Goodman, A. C., Segura, C., Jones, J. A., & Swanson, F. J. (2023). Seventy years of watershed response to floods and changing forestry practices in Western Oregon, USA. *Earth Surface Processes and Landforms*, *48*(6), 1103–1118. https://doi.org/10.1002/esp.5537

Grandi, G., & Bertuzzo, E. (2022). Catchment dissolved organic carbon transport: A modeling approach combining water travel times and reactivity continuum. *Water Resources Research*, *58*(7), e2021WR031275. https://doi.org/10.1029/2021WR031275

Guo, D., Westra, S., & Maier, H. R. (2016). An R package for modelling actual, potential and reference evapotranspiration. *Environmental Modelling and Software*, *78*, 216–224. https://doi.org/10.1016/j.envsoft.2015.12.019

Hamamoto, S., Moldrup, P., Kawamoto, K., & Komatsu, T. (2010). Excluded-volume expansion of Archie's law for gas and solute diffusivities and electrical and thermal conductivities in variably saturated porous media. *Water Resources Research*, *46*(6). https://doi.org/10.1029/2009WR008424

Hansen, M. C., Potapov, P. V., Moore, R., Hancher, M., Turubanova, S. A., Tyukavina, A., et al. (2013). High-resolution global maps of 21st-Century Forest cover change. *Science*, *342*(6160), 850–853. https://doi.org/10.1126/science.1244693

Hanson, P. J., Edwards, N. T., Garten, C. T., & Andrews, J. A. (2000). Separating root and soil microbial contributions to soil respiration: A review of methods and observations. *Biogeochemistry*, *48*(1), 115–146. https://doi.org/10.1023/a:1006244819642

Hargreaves, G. H., & Samani, Z. A. (1985). Reference crop evapotranspiration from temperature. *Applied Engineering in Agriculture*, *1*(2), 96–99. https://doi.org/10.13031/2013.26773

Harper, R. J., & Tibbett, M. (2013). The hidden organic carbon in deep mineral soils. *Plant and Soil*, *368*(1), 641–648. https://doi.org/10.1007/s11104-013-1600-9

Harris, N. L., Gibbs, D. A., Baccini, A., Birdsey, R. A., de Bruin, S., Farina, M., et al. (2021). Global maps of twenty-first century forest carbon fluxes. *Nature Climate Change*, *11*(3), 234–240. https://doi.org/10.1038/s41558-020-00976-6

Hasenmueller, E. A., Gu, X., Weitzman, J. N., Adams, T. S., Stinchcomb, G. E., Eissenstat, D. M., et al. (2017). Weathering of rock to regolith: The activity of deep roots in bedrock fractures. *Geoderma*, *300*, 11–31. https://doi.org/10.1016/j.geoderma.2017.03.020

He, Y., Cheng, W., Zhou, L., Shao, J., Liu, H., Zhou, H., et al. (2020). Soil DOC release and aggregate disruption mediate rhizosphere priming effect on soil C decomposition. *Soil Biology and Biochemistry*, *144*, 107787. https://doi.org/10.1016/j.soilbio.2020.107787

Helton, J. C., & Davis, F. J. (2003). Latin hypercube sampling and the propagation of uncertainty in analyses of complex systems. *Reliability Engineering and System Safety*, *81*(1), 23–69. https://doi.org/10.1016/S0951-8320(03)00058-9

Herndon, E. M., Dere, A. L., Sullivan, P. L., Norris, D., Reynolds, B., & Brantley, S. L. (2015). Landscape heterogeneity drives contrasting concentration–discharge relationships in shale headwater catchments. *Hydrology and Earth System Sciences*, *19*(8), 3333–3347. https://doi.org/10.5194/hess-19-3333-2015

Hertel, D., Leuschner, C., & Hölscher, D. (2003). Size and structure of fine root systems in old-growth and secondary tropical montane forests (Costa Rica). *Biotropica*, *35*(2), 143–153. https://doi.org/10.1111/j.1744-7429.2003.tb00274.x

Holl, K. D., & Brancalion, P. H. S. (2020). Tree planting is not a simple solution. *Science*, *368*(6491), 580–581. https://doi.org/10.1126/science.aba8232

Hood, E., Gooseff, M. N., & Johnson, S. L. (2006). Changes in the character of stream water dissolved organic carbon during flushing in three small watersheds, Oregon. *Journal of Geophysical Research*, *111*(G1). https://doi.org/10.1029/2005JG000082

Hotchkiss, E. R., Hall Jr, R. O., Sponseller, R. A., Butman, D., Klaminder, J., Laudon, H., et al. (2015). Sources of and processes controlling CO2 emissions change with the size of streams and rivers. *Nature Geoscience*, *8*(9), 696–699. https://doi.org/10.1038/ngeo2507

Jagodzinski, A. M., Ziółkowski, J., Warnkowska, A., & Prais, H. (2016). Tree Age effects on fine root biomass and morphology over chronosequences of Fagus sylvatica, Quercus robur and Alnus glutinosa stands. *PLoS One*, *11*(2), e0148668. https://doi.org/10.1371/journal.pone.0148668

Jarecke, K. M., Zhang, X., Keen, R. M., Dumont, M., Li, B., Sadayappan, K., et al. (2025). Woody encroachment modifies subsurface structure and hydrological function. *Ecohydrology*, *18*(2), e2731. https://doi.org/10.1002/eco.2731

Jassal, R. S., Black, T. A., Drewitt, G. B., Novak, M. D., Gaumont-Guay, D., & Nesic, Z. (2004). A model of the production and transport of CO2 in soil: Predicting soil CO2 concentrations and CO2 efflux from a forest floor. *Agricultural and Forest Meteorology*, *124*(3), 219–236. https://doi.org/10.1016/j.agrformet.2004.01.013

Johnson, M. S., Lehmann, J., Couto, E. G., Filho, J. P. N., & Riha, S. J. (2006). DOC and DIC in flowpaths of Amazonian headwater catchments with hydrologically contrasting soils. *Biogeochemistry*, *81*(1), 45–57. https://doi.org/10.1007/s10533-006-9029-3

Johnson, S., & Fredriksen, R. (2019a). *Precipitation chemistry concentrations and fluxes, HJ Andrews Experimental forest, 1969 to present. long-Term Ecological Research*. Forest Science Data Bank. https://doi.org/10.6073/pasta/2cee34b1d3c0836888444f9033c1c1c8

Johnson, S., & Fredriksen, R. (2019b). *Stream chemistry concentrations and fluxes using proportional sampling in the Andrews Experimental Forest, 1968 to present. Long-Term Ecological Research*. Forest Science Data Bank. [Database]. Retrieved from http://andlter.forestry.oregonstate.edu/data/abstract.aspx?dbcode=CF002

Johnson, S., Wondzell, S., & Rothacher, J. (2024). *Stream discharge in gaged watersheds at the HJ Andrews Experimental Forest, 1949 to present. Long-Term Ecological Research*. Forest Science Data Bank. https://doi.org/10.6073/pasta/ba33b8509dfd018f39f39f40d9f6dd7b

Johnson, S. L., Henshaw, D., Downing, G., Wondzell, S., Schulze, M., Kennedy, A., et al. (2021). Long-term hydrology and aquatic biogeochemistry data from H. J. Andrews Experimental Forest, Cascade Mountains, Oregon. *Hydrological Processes*, *35*(5), e14187. https://doi.org/10.1002/hyp.14187

Johnson, S. L., & Jones, J. A. (2000). Stream temperature responses to forest harvest and debris flows in western Cascades, Oregon. *Canadian Journal of Fisheries and Aquatic Sciences*, *57*(S2), 30–39. https://doi.org/10.1139/cjfas-57-s2-30

Jones, J. A., & Grant, G. E. (1996). Peak flow responses to clear-cutting and roads in small and large basins, Western cascades, Oregon. *Water Resources Research*, *32*(4), 959–974. https://doi.org/10.1029/95WR03493

Kaiser, K., & Guggenberger, G. (2000). The role of DOM sorption to mineral surfaces in the preservation of organic matter in soils. *Organic Geochemistry*, *31*(7), 711–725. https://doi.org/10.1016/S0146-6380(00)00046-2

Karimi, S., Seibert, J., & Laudon, H. (2022). Evaluating the effects of alternative model structures on dynamic storage simulation in heterogeneous boreal catchments. *Hydrology Research*, *53*(4), 562–583. https://doi.org/10.2166/nh.2022.121

Keller, C. K. (2019). Carbon exports from terrestrial ecosystems: A critical-zone framework. *Ecosystems*, *22*(8), 1691–1705. https://doi.org/10.1007/s10021-019-00375-9

Kerins, D., Sadayappan, K., Zhi, W., Sullivan, P. L., Williams, K. H., Carroll, R. W. H., et al. (2024). Hydrology outweighs temperature in driving production and export of dissolved carbon in a snowy Mountain catchment. *Water Resources Research*, *60*(7), e2023WR036077. https://doi.org/10.1029/2023WR036077

Kincaid, D. W., Underwood, K. L., Hamshaw, S. D., Li, L., Seybold, E. C., Stewart, B., et al. (2024). Solute export patterns across the contiguous USA. *Hydrological Processes*, *38*(6), e15197. https://doi.org/10.1002/hyp.15197

Kirchner, J. W. (2009). Catchments as simple dynamical systems: Catchment characterization, rainfall-runoff modeling, and doing hydrology backward. *Water Resources Research*, *45*(2). https://doi.org/10.1029/2008WR006912

Klaus, M. (2023). Decadal increase in groundwater inorganic carbon concentrations across Sweden. *Communications Earth and Environment*, *4*(1), 1–10. https://doi.org/10.1038/s43247-023-00885-4

Knapp, J. L. A., von Freyberg, J., Studer, B., Kiewiet, L., & Kirchner, J. W. (2020). Concentration–discharge relationships vary among hydrological events, reflecting differences in event characteristics. *Hydrology and Earth System Sciences*, *24*(5), 2561–2576. https://doi.org/10.5194/hess-24-2561-2020

Lajtha, K., & Jones, J. (2018). Forest harvest legacies control dissolved organic carbon export in small watersheds, western Oregon. *Biogeochemistry*, *140*(3), 299–315. https://doi.org/10.1007/s10533-018-0493-3

Lasaga, A. C. (2014). *Kinetic theory in the Earth sciences*. Princeton University Press. https://doi.org/10.1515/9781400864874

Laudon, H., Berggren, M., Ågren, A., Buffam, I., Bishop, K., Grabs, T., et al. (2011). Patterns and dynamics of Dissolved Organic Carbon (DOC) in boreal streams: The role of processes, connectivity, and scaling. *Ecosystems*, *14*(6), 880–893. https://doi.org/10.1007/s10021-011-9452-8

Ledesma, J. L. J., Grabs, T., Bishop, K. H., Schiff, S. L., & Köhler, S. J. (2015). Potential for long-term transfer of dissolved organic carbon from riparian zones to streams in boreal catchments. *Global Change Biology*, *21*(8), 2963–2979. https://doi.org/10.1111/gcb.12872

Lee, B. S., & Lajtha, K. (2016). Hydrologic and forest management controls on dissolved organic matter characteristics in headwater streams of old-growth forests in the Oregon Cascades. *Forest Ecology and Management*, *380*, 11–22. https://doi.org/10.1016/j.foreco.2016.08.029

Lehmann, J., & Kleber, M. (2015). The contentious nature of soil organic matter. *Nature*, *528*(7580), 60–68. https://doi.org/10.1038/nature16069

Leonard, L. T., Vanzin, G. F., Garayburu-Caruso, V. A., Lau, S. S., Beutler, C. A., Newman, A. W., et al. (2022). Disinfection byproducts formed during drinking water treatment reveal an export control point for dissolved organic matter in a subalpine headwater stream. *Water Research X*, *15*, 100144. https://doi.org/10.1016/j.wroa.2022.100144

Li, L. (2019). Watershed reactive transport. *Reviews in Mineralogy and Geochemistry*, *85*(1), 381–418. https://doi.org/10.2138/rmg.2018.85.13

Li, L. (2025). Ancient carbon released through modern rivers. *Nature*, *642*(8066), 41–42. https://doi.org/10.1038/d41586-025-01452-x

Li, L., Stewart, B., Zhi, W., Sadayappan, K., Ramesh, S., Kerins, D., et al. (2022). Climate controls on River chemistry. *Earth's Future*, *10*(6), e2021EF002603. https://doi.org/10.1029/2021EF002603

Li, S., Delgado-Baquerizo, M., Ding, J., Hu, H., Huang, W., Sun, Y., et al. (2024). Intrinsic microbial temperature sensitivity and soil organic carbon decomposition in response to climate change. *Global Change Biology*, *30*(6), e17395. https://doi.org/10.1111/gcb.17395

Lindenmayer, D., & Bowd, E. (2022). Critical ecological roles, structural attributes and conservation of old growth Forest: Lessons from a case Study of Australian Mountain ash forests. *Frontiers in Forests and Global Change*, *5*, 878570. https://doi.org/10.3389/ffgc.2022.878570

Litton, C. M., Raich, J. W., & Ryan, M. G. (2007). Carbon allocation in forest ecosystems. *Global Change Biology*, *13*(10), 2089–2109. https://doi.org/10.1111/j.1365-2486.2007.01420.x

Liu, F. (2025). Liu_etal_BioRTHBV_HJAndrews_Model_Files [Dataset]. *Zenodo*. https://doi.org/10.5281/zenodo.15098286

Lloyd, J., & Taylor, J. A. (1994). On the temperature dependence of soil respiration. *Functional Ecology*, *8*(3), 315. https://doi.org/10.2307/2389824

Mahecha, M. D., Reichstein, M., Carvalhais, N., Lasslop, G., Lange, H., Seneviratne, S. I., et al. (2010). Global convergence in the temperature sensitivity of respiration at ecosystem level. *Science*, *329*(5993), 838–840. https://doi.org/10.1126/science.1189587

Marx, A., Dusek, J., Jankovec, J., Sanda, M., Vogel, T., van Geldern, R., et al. (2017). A review of CO2 and associated carbon dynamics in headwater streams: A global perspective. *Reviews of Geophysics*, *55*(2), 560–585. https://doi.org/10.1002/2016RG000547

Mayes, M. A., Heal, K. R., Brandt, C. C., Phillips, J. R., & Jardine, P. M. (2012). Relation between soil order and sorption of dissolved organic carbon in temperate subsoils. *Soil Science Society of America Journal*, *76*(3), 1027–1037. https://doi.org/10.2136/sssaj2011.0340

McDonnell, J. J., Evaristo, J., Bladon, K. D., Buttle, J., Creed, I. F., Dymond, S. F., et al. (2018). Water sustainability and watershed storage. *Nature Sustainability*, *1*(8), 378–379. https://doi.org/10.1038/s41893-018-0099-8

McGrath, M. J., Schulte-Frohlinde, A., & Luyssaert, S. (2024). New ways for (in)validating the forest carbon neutrality hypothesis. *Global Change Biology*, *30*(1), e16982. https://doi.org/10.1111/gcb.16982

Meyer, J. L., & Tate, C. M. (1983). The effects of watershed disturbance on dissolved organic carbon dynamics of a stream. *Ecology*, *64*(1), 33–44. https://doi.org/10.2307/1937326

Meyer, J. L., Wallace, J. B., & Eggert, S. L. (1998). Leaf litter as a source of dissolved organic carbon in streams. *Ecosystems*, *1*(3), 240–249. https://doi.org/10.1007/s100219900019

Moore, G. W., Bond, B. J., Jones, J. A., Phillips, N., & Meinzer, F. C. (2004). Structural and compositional controls on transpiration in 40- and 450-year-old riparian forests in western Oregon, USA. *Tree Physiology*, *24*(5), 481–491. https://doi.org/10.1093/treephys/24.5.481

Moore, J. A. M., Sulman, B. N., Mayes, M. A., Patterson, C. M., & Classen, A. T. (2020). Plant roots stimulate the decomposition of complex, but not simple, soil carbon. *Functional Ecology*, *34*(4), 899–910. https://doi.org/10.1111/1365-2435.13510

Najjar, R. G., Herrmann, M., Cintrón Del Valle, S. M., Friedman, J. R., Friedrichs, M. A. M., Harris, L. A., et al. (2020). Alkalinity in tidal tributaries of the Chesapeake Bay. *Journal of Geophysical Research: Oceans*, *125*(1), e2019JC015597. https://doi.org/10.1029/2019JC015597

Nave, L. E., Gough, C. M., Clay, C., Santos, F., Atkins, J. W., Benjamins-Carey, S. E., et al. (2025). Carbon cycling across ecosystem succession in a north temperate forest: Controls and management implications. *Ecological Applications*, *35*(1), e70001. https://doi.org/10.1002/eap.70001

Odum, E. P. (1969). The strategy of ecosystem development. *Science*, *164*(3877), 262–270. https://doi.org/10.1126/science.164.3877.262

Okamoto, M., Nonaka, T., Ochiai, S., & Tominaga, D. (1998). Nonlinear numerical optimization with use of a hybrid Genetic Algorithm incorporating the Modified Powell method. *Applied Mathematics and Computation*, *91*(1), 63–72. https://doi.org/10.1016/S0096-3003(97)10007-8

Oliver, C., & Larson, B. (1996). Forest stand dynamics, update edition. Yale school of the environment other 1189 publications. Retrieved from https://elischolar.library.yale.edu/fes_pubs/1

Ortega, J., Bush, S. A., Segura, C., & Sullivan, P. L. (2025). Subsurface storage drives hydrologic connectivity and spatial variability in stream chemistry. *Hydrological Processes*, *39*(8), e70228. https://doi.org/10.1002/hyp.70228

Ortega, J., Segura, C., Brooks, J. R., & Sullivan, P. L. (2025). Insights into heterogeneous streamflow generation processes and water contribution in forested headwaters. *Hydrological Processes*, *39*(8), e70241. https://doi.org/10.1002/hyp.70241

Perry, T. D., & Jones, J. A. (2017). Summer streamflow deficits from regenerating Douglas-fir forest in the Pacific Northwest, USA. *Ecohydrology*, *10*(2), e1790. https://doi.org/10.1002/eco.1790

Pivovaroff, A. L., McDowell, N. G., Rodrigues, T. B., Brodribb, T., Cernusak, L. A., Choat, B., et al. (2021). Stability of tropical forest tree carbon-water relations in a rainfall exclusion treatment through shifts in effective water uptake depth. *Global Change Biology*, *27*(24), 6454–6466. https://doi.org/10.1111/gcb.15869

Pregitzer, K. S., & Euskirchen, E. S. (2004). Carbon cycling and storage in world forests: Biome patterns related to forest age. *Global Change Biology*, *10*(12), 2052–2077. https://doi.org/10.1111/j.1365-2486.2004.00866.x

Raymond, P. A., & Saiers, J. E. (2010). Event controlled DOC export from forested watersheds. *Biogeochemistry*, *100*(1), 197–209. https://doi.org/10.1007/s10533-010-9416-7

R Core Team. (2024). *R: A language and environment for statistical computing*. R Foundation for Statistical Computing.

Riebe, C. S., Hahm, W. J., & Brantley, S. L. (2017). Controls on deep critical zone architecture: A historical review and four testable hypotheses. *Earth Surface Processes and Landforms*, *42*(1), 128–156. https://doi.org/10.1002/esp.4052

Rodríguez-Cardona, B. M., Wymore, A. S., Argerich, A., Barnes, R. T., Bernal, S., Brookshire, E. N. J., et al. (2022). Shifting stoichiometry: Long-term trends in stream-dissolved organic matter reveal altered C:N ratios due to history of atmospheric acid deposition. *Global Change Biology*, *28*(1), 98–114. https://doi.org/10.1111/gcb.15965

Rodtassana, C., Unawong, W., Yaemphum, S., Chanthorn, W., Chawchai, S., Nathalang, A., et al. (2021). Different responses of soil respiration to environmental factors across forest stages in a Southeast Asian forest. *Ecology and Evolution*, *11*(21), 15430–15443. https://doi.org/10.1002/ece3.8248

Römkens, P., Hoenderboom, G., & Dolfing, J. (1999). Copper solution geochemistry in arable soils: Field observations and model application. *Journal of Environmental Quality*, *28*(3), 776–783. https://doi.org/10.2134/jeq1999.00472425002800030007x

Rose, L. A., Karwan, D. L., & Godsey, S. E. (2018). Concentration–discharge relationships describe solute and sediment mobilization, reaction, and transport at event and longer timescales. *Hydrological Processes*, *32*(18), 2829–2844. https://doi.org/10.1002/hyp.13235

Rothacher, J. (1970). Increases in water yield following clear-cut logging in the Pacific Northwest. *Water Resources Research*, *6*(2), 653–658. https://doi.org/10.1029/WR006i002p00653

Rumpel, C., & Kögel-Knabner, I. (2011). Deep soil organic matter—A key but poorly understood component of terrestrial C cycle. *Plant and Soil*, *338*(1), 143–158. https://doi.org/10.1007/s11104-010-0391-5

Ryan, K. A., Adler, T., Chalmers, A., Perdrial, J., Shanley, J. B., & Stubbins, A. (2021). Event Scale relationships of DOC and TDN fluxes in throughfall and stemflow diverge from stream exports in a forested catchment. *Journal of Geophysical Research: Biogeosciences*, *126*(7), e2021JG006281. https://doi.org/10.1029/2021JG006281

Ryan, M. G., Binkley, D., & Fownes, J. H. (1997). Age-Related decline in Forest productivity: Pattern and process. In *Advances in Ecological Research* (Eds.). M. Begon & A. H. Fitter (Vol. 27, pp. 213–262). Academic Press. https://doi.org/10.1016/S0065-2504(08)60009-4

Sadayappan, K., Stewart, B., Kerins, D., Vierbicher, A., Zhi, W., Smykalov, V. D., et al. (2024). BioRT-HBV 1.0: A biogeochemical reactive transport model at the watershed Scale. *Journal of Advances in Modeling Earth Systems*, *16*(12), e2024MS004217. https://doi.org/10.1029/2024MS004217

Sadayappan, K., Stewart, B., Kerins, D., Vierbicher, A., Zhi, W., Vis, M. J. P., et al. (2024b). Li-Reactive-Water-Group/BioRT-HBV: V-1.0 BioRT-HBV (v1.0_BioRT_HBV) [Dataset]. https://doi.org/10.5281/zenodo.10724555

Sadiq, R., & Rodriguez, M. J. (2004). Disinfection by-products (DBPs) in drinking water and predictive models for their occurrence: A review. *Science of The Total Environment*, *321*(1), 21–46. https://doi.org/10.1016/j.scitotenv.2003.05.001

Sarai, S.-S., De Jong, B. H. J., Esperanza, H.-L., Jorge, M.-V., Danilo, M.-R., & Aryal, D. R. (2022). Fine root biomass stocks but not the production and turnover rates vary with the age of tropical successional forests in Southern Mexico. *Rhizosphere*, *21*, 100474. https://doi.org/10.1016/j.rhisph.2022.100474

Schmidt, M. W. I., Torn, M. S., Abiven, S., Dittmar, T., Guggenberger, G., Janssens, I. A., et al. (2011). Persistence of soil organic matter as an ecosystem property. *Nature*, *478*(7367), 49–56. https://doi.org/10.1038/nature10386

Sebestyen, S. D., Boyer, E. W., & Shanley, J. B. (2009). Responses of stream nitrate and DOC loadings to hydrological forcing and climate change in an upland forest of the northeastern United States. *Journal of Geophysical Research*, *114*(G2). https://doi.org/10.1029/2008JG000778

Segura, C., Bladon, K. D., Hatten, J. A., Jones, J. A., Hale, V. C., & Ice, G. G. (2020). Long-term effects of forest harvesting on summer low flow deficits in the Coast Range of Oregon. *Journal of Hydrology*, *585*, 124749. https://doi.org/10.1016/j.jhydrol.2020.124749

Seibert, J. (2000). Multi-criteria calibration of a conceptual runoff model using a genetic algorithm. *Hydrology and Earth System Sciences*, *4*(2), 215–224. https://doi.org/10.5194/hess-4-215-2000

Seibert, J., & McDonnell, J. J. (2010). Land-cover impacts on streamflow: A change-detection modelling approach that incorporates parameter uncertainty. *Hydrological Sciences Journal*, *55*(3), 316–332. https://doi.org/10.1080/02626661003683264

Seibert, J., & Vis, M. J. P. (2012). Teaching hydrological modeling with a user-friendly catchment-runoff-model software package. *Hydrology and Earth System Sciences*, *16*(9), 3315–3325. https://doi.org/10.5194/hess-16-3315-2012

Smiley, B. P., & Trofymow, J. A. (2017). Historical effects of dissolved organic carbon export and land management decisions on the watershed-scale forest carbon budget of a coastal British Columbia douglas-fir-dominated landscape. *Carbon Balance and Management*, *12*(1), 15. https://doi.org/10.1186/s13021-017-0083-z

Soil Survey Staff. (2024). *Web Soil Survey*. US Department of Agriculture, Natural Resources Conservation Service. Available online at: http://websoilsurvey.sc.egov.usda.gov/

Soulsby, C., Piegat, K., Seibert, J., & Tetzlaff, D. (2011). Catchment-scale estimates of flow path partitioning and water storage based on transit time and runoff modelling. *Hydrological Processes*, *25*(25), 3960–3976. https://doi.org/10.1002/hyp.8324

Stewart, B., & Li, L. (2025). Mechanisms underlying near-universal export patterns of dissolved carbon from land to Rivers. *Global Biogeochemical Cycles*, *39*(8), e2024GB008361. https://doi.org/10.1029/2024GB008361

Stewart, B., Shanley, J. B., Kirchner, J. W., Norris, D., Adler, T., Bristol, C., et al. (2022). Streams as mirrors: Reading subsurface water chemistry from stream chemistry. *Water Resources Research*, *58*(1), e2021WR029931. https://doi.org/10.1029/2021WR029931

Stewart, B., Shanley, J. B., Matt, S., Seybold, E. C., Kincaid, D. W., Vierbicher, A., et al. (2024). Illuminating the "Invisible": Substantial deep respiration and lateral export of dissolved carbon from beneath soil. *Water Resources Research*, *60*(6), e2023WR035940. https://doi.org/10.1029/2023WR035940

Stewart, B., Zhi, W., Sadayappan, K., Sterle, G., Harpold, A., & Li, L. (2022). Soil CO2 controls short-term variation but climate regulates long-term mean of riverine inorganic carbon. *Global Biogeochemical Cycles*, *36*(8), e2022GB007351. https://doi.org/10.1029/2022GB007351

Stolze, L., Arora, B., Dwivedi, D., Steefel, C. I., Bandai, T., Wu, Y., & Nico, P. (2024). Climate forcing controls on carbon terrestrial fluxes during shale weathering. *Proceedings of the National Academy of Sciences*, *121*(27), e2400230121. https://doi.org/10.1073/pnas.2400230121

Su, H., Cheng, L., Wu, Y., Qin, S., Liu, P., Zhang, Q., et al. (2023). Extreme storm events shift DOC export from transport-limited to source-limited in a typical flash flood catchment. *Journal of Hydrology*, *620*, 129377. https://doi.org/10.1016/j.jhydrol.2023.129377

Sullivan, P. L., Billings, S. A., Hirmas, D., Li, L., Zhang, X., Ziegler, S., et al. (2022). Embracing the dynamic nature of soil structure: A paradigm illuminating the role of life in critical zones of the Anthropocene. *Earth-Science Reviews*, *225*, 103873. https://doi.org/10.1016/j.earscirev.2021.103873

Sullivan, P. L., Genereux, D. P., Brookfield, A. E., Rempe, D., Stotler, R. L., Barnard, H. R., et al. (2024). Groundwater—The dynamic base of the CZ. In T. White & A. Provenzale (Eds.), *Critical Zone and ecosystem dynamics* (pp. 109–148). Springer Nature. https://doi.org/10.1007/978-3-031-69076-1_5

Sullivan, P. L., Hynek, S. A., Gu, X., Singha, K., White, T., West, N., et al. (2016). Oxidative dissolution under the channel leads geomorphological evolution at the shale hills catchment. *American Journal of Science*, *316*(10), 981–1026. Scopus. https://doi.org/10.2475/10.2016.02

Swanson, F. J. (1975). *Geology and geomorphology of the H.J. Andrews Experimental Forest, Western cascades, Oregon. Pacific Northwest Forest and range experiment station, Forest service*. U.S. Department of Agriculture.

Tank, S. E., Fellman, J. B., Hood, E., & Kritzberg, E. S. (2018). Beyond respiration: Controls on lateral carbon fluxes across the terrestrial-aquatic interface. *Limnology and Oceanography Letters*, *3*(3), 76–88. https://doi.org/10.1002/lol2.10065

Tao, Z., Neil, E., & Si, B. (2021). Determining deep root water uptake patterns with tree age in the Chinese loess area. *Agricultural Water Management*, *249*, 106810. https://doi.org/10.1016/j.agwat.2021.106810

Tetzlaff, D., Birkel, C., Dick, J., Geris, J., & Soulsby, C. (2014). Storage dynamics in hydropedological units control hillslope connectivity, runoff generation, and the evolution of catchment transit time distributions. *Water Resources Research*, *50*(2), 969–985. https://doi.org/10.1002/2013WR014147

Tetzlaff, D., Seibert, J., McGuire, K. J., Laudon, H., Burns, D. A., Dunn, S. M., & Soulsby, C. (2009). How does landscape structure influence catchment transit time across different geomorphic provinces? *Hydrological Processes*, *23*(6), 945–953. https://doi.org/10.1002/hyp.7240

Torres, M. A., West, A. J., & Clark, K. E. (2015). Geomorphic regime modulates hydrologic control of chemical weathering in the Andes–Amazon. *Geochimica et Cosmochimica Acta*, *166*, 105–128. https://doi.org/10.1016/j.gca.2015.06.007

Trumbore, S., Da Costa, E. S., Nepstad, D. C., Barbosa De Camargo, P., Martinelli, L. A., Ray, D., et al. (2006). Dynamics of fine root carbon in Amazonian tropical ecosystems and the contribution of roots to soil respiration. *Global Change Biology*, *12*(2), 217–229. https://doi.org/10.1111/j.1365-2486.2005.001063.x

Tune, A. K., Druhan, J. L., Wang, J., Bennett, P. C., & Rempe, D. M. (2020). Carbon dioxide production in bedrock beneath soils substantially contributes to Forest carbon cycling. *Journal of Geophysical Research: Biogeosciences*, *125*(12), e2020JG005795. https://doi.org/10.1029/2020JG005795

Tuswa, N., Bugan, R. D. H., Mapeto, T., Jovanovic, N., Gush, M., Kapangaziwiri, E., et al. (2019). The impacts of commercial plantation forests on groundwater recharge: A case study from George (Western Cape, South Africa). *Physics and Chemistry of the Earth, Parts A/B/C*, *112*, 187–199. https://doi.org/10.1016/j.pce.2018.12.006

UNEP, and FAO. (2020). *The State of the World's forests 2020*. FAO and UNEP. Retrieved from https://openknowledge.fao.org/handle/20.500.14283/ca8642en

Valett, H. M., Crenshaw, C. L., & Wagner, P. F. (2002). Stream nutrient uptake, Forest succession, and biogeochemical theory. *Ecology*, *83*(10), 2888–2901. https://doi.org/10.1890/0012-9658(2002)083%255B2888:SNUFSA%255D2.0.CO;2

Vitousek, P. M., & Reiners, W. A. (1975). Ecosystem succession and nutrient retention: A Hypothesis. *BioScience*, *25*(6), 376–381. https://doi.org/10.2307/1297148

Waichler, S. R., Wemple, B. C., & Wigmosta, M. S. (2005). Simulation of water balance and forest treatment effects at the H.J. Andrews Experimental Forest. *Hydrological Processes*, *19*(16), 3177–3199. https://doi.org/10.1002/hyp.5841

Wallin, M. B., Grabs, T., Buffam, I., Laudon, H., Ågren, A., Öquist, M. G., & Bishop, K. (2013). Evasion of CO2 from streams—The dominant component of the carbon export through the aquatic conduit in a boreal landscape. *Global Change Biology*, *19*(3), 785–797. https://doi.org/10.1111/gcb.12083

Weisberg, P. J., & Swanson, F. J. (2003). Regional synchroneity in fire regimes of western Oregon and Washington, USA. *Forest Ecology and Management*, *172*(1), 17–28. https://doi.org/10.1016/S0378-1127(01)00805-2

Wen, H., Sullivan, P. L., Billings, S. A., Ajami, H., Cueva, A., Flores, A., et al. (2022). From Soils to streams: Connecting terrestrial carbon transformation, chemical weathering, and solute export across hydrological regimes. *Water Resources Research*, *58*(7), e2022WR032314. https://doi.org/10.1029/2022WR032314

Wolf-Gladrow, D. A., Zeebe, R. E., Klaas, C., Körtzinger, A., & Dickson, A. G. (2007). Total alkalinity: The explicit conservative expression and its application to biogeochemical processes. *Marine Chemistry*, *106*(1), 287–300. https://doi.org/10.1016/j.marchem.2007.01.006

Wymore, A. S., Brereton, R. L., Ibarra, D. E., Maher, K., & McDowell, W. H. (2017). Critical zone structure controls concentration-discharge relationships and solute generation in forested tropical montane watersheds. *Water Resources Research*, *53*(7), 6279–6295. https://doi.org/10.1002/2016WR020016

Xiao, D., Brantley, S. L., & Li, L. (2021). Vertical connectivity regulates water transit time and chemical weathering at the hillslope Scale. *Water Resources Research*, *57*(8), e2020WR029207. https://doi.org/10.1029/2020WR029207

Xiao, D., Shi, Y., Brantley, S. L., Forsythe, B., DiBiase, R., Davis, K., & Li, L. (2019). Streamflow generation from catchments of contrasting lithologies: The role of soil properties, topography, and catchment size. *Water Resources Research*, *55*(11), 9234–9257. https://doi.org/10.1029/2018WR023736

Xu, S., Li, S.-L., Bufe, A., Klaus, M., Zhong, J., Wen, H., et al. (2024). Escalating carbon export from high-elevation Rivers in a warming climate. *Environmental Science & Technology*, *58*(16), 7032–7044. https://doi.org/10.1021/acs.est.3c06777

Yan, Z., Bond-Lamberty, B., Todd-Brown, K. E., Bailey, V. L., Li, S., Liu, C., & Liu, C. (2018). A moisture function of soil heterotrophic respiration that incorporates microscale processes. *Nature Communications*, *9*(1), 2562. https://doi.org/10.1038/s41467-018-04971-6

Yanai, R. D., Park, B. B., & Hamburg, S. P. (2006). The vertical and horizontal distribution of roots in northern hardwood stands of varying age. *Canadian Journal of Forest Research*, *36*(2), 450–459. https://doi.org/10.1139/x05-254

Zarnetske, J. P., Bouda, M., Abbott, B. W., Saiers, J., & Raymond, P. A. (2018). Generality of hydrologic transport limitation of watershed organic carbon flux across ecoregions of the United States. *Geophysical Research Letters*, *45*(21). https://doi.org/10.1029/2018GL080005

Zhang, Z. Q., Evaristo, J., Li, Z., Si, B. C., & McDonnell, J. J. (2017). Tritium analysis shows apple trees may be transpiring water several decades old. *Hydrological Processes*, *31*(5), 1196–1201. https://doi.org/10.1002/hyp.11108

Zhao, L. Y. L., Schulin, R., Weng, L., & Nowack, B. (2007). Coupled mobilization of dissolved organic matter and metals (Cu and Zn) in soil columns. *Geochimica et Cosmochimica Acta*, *71*(14), 3407–3418. https://doi.org/10.1016/j.gca.2007.04.020

Zhi, W., & Li, L. (2020). The shallow and deep Hypothesis: Subsurface vertical chemical contrasts shape nitrate export patterns from different land uses. *Environmental Science & Technology*, *54*(19), 11915–11928. https://doi.org/10.1021/acs.est.0c01340

Zhi, W., Li, L., Dong, W., Brown, W., Kaye, J., Steefel, C., & Williams, K. H. (2019). Distinct source water chemistry shapes contrasting concentration-discharge patterns. *Water Resources Research*, *55*(5), 4233–4251. https://doi.org/10.1029/2018WR024257

Zhou, T., Shi, P., Hui, D., & Luo, Y. (2009). Global pattern of temperature sensitivity of soil heterotrophic respiration (Q10) and its implications for carbon-climate feedback. *Journal of Geophysical Research*, *114*(G2). https://doi.org/10.1029/2008JG000850